MECHANICAL

TECHNOLOGY

INCORPORATED

MTI-65TR47

AN EXPERIMENTAL STUDY OF FLOW PHENOMENA IN THE FEEDING REGION OF AN EXTERNALLY PRESSURIZED GAS BEARING

by

J. H. Vohr

Contract No. Nonr-3730(00)

NO. MTI-65TR47

DATE: July 21, 1966

TECHNICAL REPORT

AN EXPERIMENTAL STUDY OF FLOW PHENOMENA IN THE FEEDING REGION OF AN EXTERNALLY PRESSURIZED GAS BEARING

by

J. H. Vohr

J. H. Vohr

Author (s)

Carlo H. T. Pan

Approved

Approved

Prepared under

Contract Nonr-3730(00)
Task NR 061-131

Prepared for

DEPARTMENT OF DEFENSE
ATOMIC ENERGY COMMISSION
NATIONAL AERONAUTICS AND SPACE ADMINISTRATION

Administered by

OFFICE OF NAVAL RESEARCH
Department of the Navy

MTI
MECHANICAL TECHNOLOGY INCORPORATED
MTI

968 ALBANY - SHAKER ROAD — LATHAM, NEW YORK — PHONE 785-0922

TABLE OF CONTENTS

INTRODUCTION

To determine the performance of an externally pressurized fluid film bearing, it is necessary to be able to calculate the pressure loss from supply reservoir to ambient conditions as a function of the mass flow rate through the bearing. In general, there are three distinct sources of pressure loss. These are illustrated in the schematic diagram shown in Fig. 1. One source of loss is the laminar viscous pressure loss in the bearing film. A second is the pressure loss due to a flow restriction, commonly an orifice, placed at the entrance to the bearing. A third possible source of pressure loss is the so-called "inherent compensation loss". This is the loss associated with the entrance of flow into the bearing film from a feeding hole located in the bearing. Generally speaking, viscous film pressure loss can be calculated with good accuracy. However, calculations of pressure loss due to orifice restrictions in the bearing are much less reliable. This is because the latter calculations are usually made for the situation where the orifice is discharging directly to the atmosphere, whereas the orifice actually discharges into a feeding hole in the bearing. As will be shown in this report, the characteristics of an orifice when it is discharging into a feeding hole can be quite different than when it is discharging to atmosphere due to the occurrence of pressure recovery in the feeding hole.

There is also considerable uncertainty involved in the calculation of inherent compensation loss. Usually, the minimum throat area at the entrance to the bearing film is treated as an orifice with variable area, and inherent compensation losses are

calculated using standard orifice coefficients. Often this approach is quite satisfactory, since inherent compensation is often a minor effect, and miscalculation of it may introduce little error into the determination of overall bearing performance. However, there are times when inherent compensation restriction is important. For example, pneumatic hammer instability considerations can make it desirable to design bearings relying solely on inherent compensation for stiffness rather than on fixed orifice restriction. In such cases, data on film entrance loss is necessary for accurate calculation of bearing performance. To this writer's knowledge, such data are almost totally lacking in the literature. Studies have been made on entrance effects in externally pressurized bearings (Ref. 1 and 2) but these have generally concentrated on the problem of supersonic flow and shocks in the vicinity of the feeding hole.

This report describes some ~~recent~~ measurements made of film entrance losses for a circular, externally pressurized, gas bearing under subsonic flow conditions. The nature of the flow in the entrance region was studied by means of pressure profile measurements. Measurements were made of the recovery of pressure downstream of an orifice discharging into the bearing feeding hole and of the influence of this orifice on film entrance pressure loss. The significance of these various phenomena on bearing performance was demonstrated by an illustrative calculation for a typical bearing.

DESCRIPTION OF THE TEST APPARATUS

A schematic drawing of the test bearing used is shown in Fig.2 and a photograph of the bearing is shown in Fig. 3. The bottom plate was made of hardened steel, chrome-plated and lapped flat to within 10 microinches. A 0.005 inch diameter pressure tap hole was drilled in the plate before it was hardened. Situated beneath this pressure tap hole was a consolidated Electrodynamic type 4-312002, unidirectional, differential pressure transducer with a range of 0 - 10 psi.

The top plate of the test bearing was made of brass with an attached disk of hardened steel for the bearing surface. This bearing surface was two inches in diameter and was also chrome plated and lapped flat to within 10 microinches. The gas supply line was a flexible rubber hose, 11/32 inches I.D., which ended in a 1/2 inch diameter supply chamber in the top plate of the bearing. At the bottom of this supply chamber was situated a thin, brass orifice plate with a .061 $\pm$ .001 inch diameter hole. This orifice plate could be removed entirely or replaced with other plates having different diameter holes. The diameter of the 61 mil hole in the orifice plate was measured with a Bausch & Lomb Stereoscope microscope using an indicating eyepiece. Below the orifice was a feeding hole 0.240 $\pm$ .005 inches in depth and 0.200 $\pm$ .001 inches in diameter. The diameter of the feeding hole was determined with the microscope mentioned above. The edge of the feeding hole at the bearing surface was uniformly sharp and free of burrs as determined by careful study through the microscope.

The top plate of the bearing was supported on three legs consisting of standard micrometer heads with minimum graduations of 0.1 mils. For each experimental run, the clearance between the top and bottom bearing surfaces was set in the following way. First the micrometer legs were retracted so that the top bearing surface rested on the bottom bearing surface. This was done while a leakage of flow

was passing through the bearing so as to remove minute foreign particles from the bearing clearance. With the bearing surfaces at zero clearance, each micrometer leg was lowered in turn until it contacted the bottom bearing surface. This established the zero setting for each leg. Starting from the zero point, each leg was then set to the desired clearance.

Before any pressure profile measurements were made, some time was spent checking the accuracy to which the bearing clearance could be set by means of the micrometer legs. The checking was done with a capacitance probe set in a recess in the surface of the bottom bearing plate. This probe was sensitive to the changes in clearances on the order of 0.1×10^{-3} inches. It was determined with this probe that clearance could be set with the micrometer legs to within an accuracy of $\pm 0.1 \times 10^{-3}$ inches. Subsequent comparisons of measured pressure profiles with predicted profiles bore out the conclusion that clearances could be set to this accuracy. As will be pointed out later in the discussion of experimental results, the actual clearance in the bearing seemed to be consistently about 0.08×10^{-3} inches greater than the clearance set by the micrometer legs. This could have been due to there being a slight residual clearance between the bearing surfaces when they were in contact, possibly as a result of minute particles in the clearance space.

The gas used in the experiments was bottled nitrogen. Before entering the bearing, the gas passed successively through a hi-pressure regulator, a Norgren air-line filter, a Moore Nullmatic pressure regulator for fine control of flow, and then through a glass bead packed column flow meter (to be described below). The supply pressure at the entrance to the bearing was measured by means of a mercury-filled "U"-tube manometer one tube of which was open to atmosphere. This manometer could easily be read to an accuracy of $\pm$ .05 inches which corresponded to an accuracy in pressure of $\pm$ .025 psi.

As noted above, flow was measured by means of a packed column glass bead flow meter. This flow meter consisted of a circular right cylinder 2 7/8 inches I.D. x 9 1/2 inches in length packed with spherical glass beads having an average diameter of 0.02 inches. The beads were kept in place by fine mesh stainless steel screening. The nitrogen flow entered this meter at the top, flowed down through the column of glass beads, and left the flow meter at the bottom. Because the flow through the column of beads was laminar, the pressure drop over the column was linearly proportional to the volume flow rate (provided the change in pressure was small compared with the pressure level.) The pressure drop across the flow meter was measured with an inclined manometer capable of measuring a total pressure drop of 6 inches H_2O in increments of 0.01 inch H_2O. The flow meter was calibrated by discharging the flow into a 50 gallon drum inverted in a larger drum full of water. The pressure inside the inverted drum was kept constant at ambient pressure by counterbalancing the weight of the drum. As water was displaced from the inverted drum by incoming nitrogen, the level of the drum rose and the rate of increase of the level provided a measure of volume flow rate. The results of the calibration of the packed column flow meter are shown in Fig.4. One can see that all the calibration points lie within 0.1 $in.^3/sec.$ of the straight calibration line. Since the minimum flow rates measured were on the order of 3 $in.^3/sec.$, the packed column flow meter was considered to be accurate to within $\pm$ 3 %.

Other investigators (Ref. 2) have reported experiencing difficulties with the packed column type of flow meter with respect to the calibration changing unpredictably with use. No such difficulty was encountered in the present work. Although calibration of the packed column flow meter was not checked after the experiments were completed, each pressure profile measured was checked against

theoretical predictions using measured values of flow rate and there was never any indication that the calibration of the flow meter had changed.

The pressure profiles in the bearing film were measured by connecting the Consolidated Electrodynamics pressure transducer to a Baldwin-Lima-Hamilton, SR-4, Strain indicator. This arrangement was first calibrated against a Barton, model 227, 10 psi, differential pressure gage and the transducer was found to have a response that was linear with pressure to within .05 psi (the rated accuracy of the gage) over the 10 psi range. A second and more exacting calibration of the pressure transducer was made with the transducer installed in the test bearing. In this calibration, the top plate of the bearing was centered over the pressure tap hole and set at zero clearance so that the pressure transducer sensed the supply pressure in the feeding hole (the orifice plate was removed from the bearing.) The pressure transducer was then calibrated vs. the mercury manometer used to measure supply pressure. The transducer was found to have a response linear with pressure within $\pm$ 025 psi over the range 0 to 4.3 psi, 4.3 psi being the limiting feeding hole pressure at which the bearing began to float. The calibration curve for the pressure transducer is shown in Fig.5 .

In order to measure pressure profiles along the bearing film, the bearing top plate was traversed along a diameter over the pressure tap hole in the bottom plate. This was accomplished by means of a horizontal micrometer head which pushed the bearing top plate along the surface of the bottom plate. A metal guide plate, lapped flat along a side and mounted on the surface of the bottom plate, was used to direct the top plate in its traverse so as to ensure that the center of the feeding hole passed directly over the pressure tap. This guide plate and the micrometer head used for the bearing traverse can be seen in Fig.3 . The chrome bearing surface of the bottom plate was sufficiently hard so that it was not scratched by the micrometer legs when the top plate was being traversed.

EXPERIMENTAL RESULTS

Measurement of Inherent Compensation Pressure Loss

The first series of measurements made in this study were to determine the entrance or "inherent compensation" pressure loss for the situation where no orifice is present in the bearing. A typical pressure profile for this situation is shown in Fig.6 *. Across the feeder hole the profile is flat and the pressure is equal to supply pressure. Right at the entrance to the bearing film the pressure profile has a very sharp depression, indicative of a vena contracta. A few hundredths of an inch away from the entrance, much of the dynamic pressure at the vena contracta has been recovered and the pressure profile begins to approach the dashed theoretical curve given by Eq. 1 below.**

$$p^2 - p_a^2 = \frac{12\mu \; Q_s \; P_s}{\pi h^3} \ln R/r \quad \ldots\ldots\ldots\ldots\ldots\ldots \quad (1)$$

where

P = pressure, lb/in^2

P_a = ambient pressure lb/in^2

μ = fluid viscosity $\frac{lb - sec}{in^2}$

Q_s = volume flow of gas at supply pressure, $in^3/sec.$

P_s = supply pressure, lb/in^2

h = bearing film clearance, in.

---

* The abscissa in figure 6 is the traverse position x as read off the traversing micrometer head. The position r = 0 at the center of the bearing occurs at x = 1.252 inches.

** For a derivation of Eq. 1, See Ref. 3.

R = radius of bearing, in.

r = radial coordinate measured from center of bearing, in.

Eq. (1) is derived under the usual fluid film lubrication assumptions, i.e. isothermal ideal gas as a lubricant, neglect of inertia terms compared with viscous terms in the equation of motion, etc. In the region $0.3 \leq r \leq 0.9$, the discrepancy between Eq. (1) and the measured pressure distribution is due mainly to the effect of inertia terms. This discrepancy can be accounted for quite accurately by subtracting the quantity $1.2\rho V_m^2/2$ for the pressure P given by Eq. (1). (ρ = local density of the flow and V_m = mean flow velocity.) This quantity represents, approximately, the mean dynamic pressure of the flow and is derived by integrating the quantity $\rho V^2/2$ across the bearing film assuming a parabolic velocity profile in the flow. Values of pressure corrected for the effect of dynamic pressure are plotted as X's in Fig. 6. As can be seen, these corrected values of pressure are in excellent agreement with measured values.

In the region $0.9 \leq r \leq 1.0$, the correction for the dynamic pressure of the flow was generally negligible and Eq. (1) should provide an accurate representation of the measured pressure profile. However, when measured values of clearance and flow rate were substituted into Eq. (1), the predicted pressure profile was slightly higher than the measured one. To bring the measured and predicted profiles into agreement, it was necessary to use a value of h in Eq. (1) that was consistently about 0.08×10^{-3} inches greater than the measured value. The need for this small correction could be explained by the existence of a small residual clearance between the top and the bottom bearing surface when the micrometer legs of the test rig were set at zero. In any case, the correction is a small one,

amounting to only 4% of the smallest clearance at which tests were run (2 mils). All of the theoretical curves shown in this report were calculated using corrected values of h.

The measured total pressure loss from the feeder hole to the outer edge of the bearing in Fig. 5 is $P_s - P_a$. The theoretical total pressure loss, assuming that only viscous forces were significant in the bearing film, would be $P_i - P_a$ where P_i is the pressure at the edge of the feeding hole as determined from equation (1), i.e.

$$P_i^2 - P_a^2 = \frac{12\mu\, Q_s P_s}{\pi h^3} \ln (R/r_i) \quad \ldots\ldots\ldots\ldots\ldots\ldots \quad (2)$$

where r_i = radius of feeding hole. It can be seen in Fig 6 that P_s is significantly greater than P_i. The difference between P_s and P_i was taken to be the pressure loss associated with entrance of the flow into the bearing clearance. In Figs. 7 through 9 are shown various representative pressure profiles measured at different clearances and flow rates with no orifice restriction in the bearing. In each case, one can note the magnitude of the entrance loss, $P_s - P_i$.

In keeping with usual practice in correlating the pressure loss associated with the entrance of flow into pipes, etc., values of $P_s - P_i$ were correlated in terms of a loss coefficient, K, multiplying the dynamic pressure at the entrance to the bearing film. This entrance dynamic pressure, denoted as P_{dyn}, was calculated from compressible flow equations under the assumption that the flow completely filled the bearing clearance at the entrance to the bearing film and that the flow underwent an isentropic acceleration starting from stagnation conditions in the feeder hole. The procedure for calculating P_{dyn} is described in Appendix A. $P_s - P_i$, the

entrance pressure loss is therefore given by

$$P_s - P_i = K P_{dyn} \quad \ldots\ldots\ldots\ldots\ldots\ldots\ldots\ldots\ldots\ldots \quad (3)$$

A total of twenty measurements of entrance pressure loss were made with no orifice restriction in the bearing. These data, plotted in terms of the entrance loss coefficient K vs. the film entrance Reynolds number $Re = \dot{m}/\pi r_i \mu$, are shown in Fig. 10. The data shows some scatter due to the fact that entrance pressure loss is measured as the difference between P_s and P_i, and a slight error in the calculation of P_i can produce a very large error in the quantity $P_s - P_i$. In spite of the scatter, the data show a clear dependence on the film entrance Reynolds number.

It was anticipated that K might depend on the ratio h/r_i and also on the Mach number at the entrance to the bearing film. Within the range of the present test conditions, no significant dependence of K on these parameters was observed. In the present tests, entrance Mach numbers were always less than 0.40. At these relatively low Mach numbers, the effect of compressibility should be fairly negligible. At higher Mach numbers, a dependence of K on Mach number would be expected.

In Fig. 11 is shown a comparison between the experimental curve of K vs. R_e obtained in the present work and some recent data on entrance effects in a circular thrust bearing with a sharp-edged supply hole obtained at the Franklin Institute Research Laboratory (Ref. 2). In order to compare the Franklin data with those obtained in the present work, it was necessary to reduce the Franklin data to the form of entrance loss coefficients. The test apparatus used at Franklin was run at much smaller clearances than was the MTI apparatus. However, the range of h/r_i was nearly the same in both investigations. As can be seen in Fig. 11, the Franklin data taken in the range $2 \times 10^{-2} \leq h/r_i \leq 8 \times 10^{-2}$ (the range investigated by MTI) lie near the experimental curve obtained in the present work. However, the two Franklin data points

shown for the case $h/r_i = 16 \times 10^{-2}$ (1.6 mils clearance) lie considerably above the MTI curve. These higher values of K may indicate a dependence of K on h/r_i at larger values of h/r_i. There is also a possibility that these higher values of K may be due to there having been some shock phenomena associated with these particular tests, since these particular tests were run at just below "choked" flow conditions.

Measurement of Orifice Characteristics

Having determined the loss coefficients for flow entering the bearing film from the feeding hole, we next determined the pressure loss vs. flow characteristics for the orifice that was to be installed in the bearing. An expression for the pressure loss across the orifice can be obtained by writing the ideal isentropic equation for flow through an orifice and multiplying this expression by an empirical vena contracta coefficient α and an empirical "efficiency" coefficient η. The latter coefficient accounts for the fact that the actual flow would not be exactly isentropic. The expression obtained is

$$\frac{\dot{m}}{g_c} = \alpha \sqrt{\eta}\, a \left\{ P_s \frac{\rho_s}{g_c} \left(\frac{P_c}{P_s}\right)^{\frac{2}{k}} \left(\frac{k}{k-1}\right) \left[1 - \frac{P_c}{P_s}^{\frac{k-1}{k}}\right] \right\}^{1/2} \quad \ldots\ldots\ldots\ldots \quad (4)$$

where

P_c = static pressure at vena contracta downstream of orifice, lb/in^2.

$\dot{m}$ = mass flow rate, lb/sec.

a = orifice flow area, in^2.

k = ratio specific heats = 1.4 for nitrogen.

g_c = gravitational constant = 386 in/sec^2.

ρ_s = supply density, lb/in^3.

P_s = supply pressure, lb/in^2

From the standpoint of physical understanding, Eq. (4) is the best way of relating flow through the orifice to the parameters affecting it. However, for simplicity, in this study we chose to use the following "working" equation for compressible flow through the orifice.

$$\frac{\dot{m}}{g_c} = \sqrt{2}\, a\, K_o\, Y_1 \sqrt{\frac{\rho_s}{g_c}\,(P_s - P_c)} \quad \ldots\ldots\ldots\ldots\ldots\ldots\ldots\ldots (5)$$

The factor K_o in equation (5) is the vena contracta orifice coefficient for incompressible flow while Y_1, called the expansion factor, is an empirical factor to adjust the equation for compressible flow. For square edged orifices, K_o is usually about 0.61 while Y_1 is a linear function of the pressure ratio across the orifice varying between 1.0 for $P_c/P_s = 1$ to about 0.87 for $P_c/P_s = 0.6$. To determine K_o and Y_1 for the particular orifice used in our tests, the orifice was installed in the bearing and allowed to discharge directly to atmosphere. The measured values of K_o and Y_1 are shown in Fig. 12 and 13. K_o is plotted as a function of Re', the Reynolds number in the supply line feeding the orifice. One can note that for Re' $>$ 2,250 K_o is constant at a value of 0.63 whereas for Re' $<$ 2,250 K_o is a mild function of upstream Reynolds number. This is typical of orifice discharge coefficients. The dependance of Y_1 on P_c/P_s shown in Fig. 13 also represents typical behavior for this coefficient.

With pressure vs. flow characteristics for the orifice discharging to atmosphere determined,the next step in the tests was to measure the orifice characteristics with a bearing clearance sufficiently large such that viscous pressure losses and entrance pressure losses associated with flow in the bearing film would be negligible. In this case, the high velocity flow from the orifice impinged upon the surface of the bottom plate of the bearing rather than discharing directly to atmosphere. It was anticipated that as a result of this impingement, a significant fraction of the dynamic pressure of the orifice jet would be recovered.

The first measurements were made at a bearing clearance of ten mils. A characteristic

pressure profile measured across the orifice jet is shown in Fig. 14. The geometry of the orifice, feeding hole and bearing film are also shown drawn to scale. Directly under the center of the orifice, the pressure tap senses nearly the full supply pressure. Radially outward from the center of the feeding hole, the measured pressure decreases until it reaches a minimum at $r \tilde{=} 0.072$. This minimum is nearly equal to P_c, the downstream pressure that would result if the orifice jet were discharging to atmosphere.

Moving further outward from $r = 0.072$, the high velocity jet from the orifice, turned by the bottom plate, begins to decelerate and recover some of its dynamic pressure. Note that a substantial amount of this recovery occurs within the feeding hole. At the edge of the feeding hole ($r = 0.10$) the flow from the orifice seems to enter the thin bearing film very smoothly with no evidence of it being obstructed by the sharp edge of the feeding hole. This indicates that most of the flow from the orifice must be spread out in a thin layer along the surface at the bottom of the feeding hole. This layer of flow must be on the order of 10 mils thick or less at the edge of the feeding hole. If the layer were thicker, the flow would have to accelerate upon entering the bearing film and this would have shown up as a depression in the pressure profile at the entrance to the bearing film.

At the clearance of 10 mils, the viscous pressure loss in the bearing film is negligible compared with the difference $P_s - P_a$. Also, as pointed out above, there appear to be no entrance losses. Therefore, $P_s - P_a$, the total pressure loss from the supply line to the outside of the bearing, should be entirely orifice loss. As was anticipated, this orifice loss was significantly less than $P_s - P_c$, the loss that would have occurred had the orifice exhausted directly to atmosphere. The difference between the quantity $(P_s - P_c)$ and $(P_s - P_a)$, divided by $(P_s - P_c)$, represents the fraction of the orifice "loss" that is recovered due to impingement

on the bottom plate. This is expressed in terms of a recovery factor β, where

$$\beta = \frac{P_a - P_c}{P_s - P_c} \quad \ldots\ldots\ldots\ldots\ldots\ldots\ldots\ldots\ldots\ldots\ldots\ldots \quad (6)$$

Measurements of β were made at different flow rates at bearing clearances of 10 mils and 15 mils. The results are plotted in Fig. 15 in terms of (1-β) vs. P_c/P_s. Re', the Reynolds number in the supply line, is also indicated for some of the data. For values of P_c/P_s less than 0.95 (Re' > 2000) the measured values of (1 - β) all lie very consistently near 0.741. As would be expected, there is no difference between measurements taken at 10 mils and at 15 mils. This is because the recovery of dynamic pressure in the orifice jet should depend on the distance from the orifice to the bottom of the feeding hole, and a difference of 5 mils in this height is negligible. One would also expect that the orifice pressure recovery should remain the same when clearance is decreased from 10 mils, at least until the point is reached where the sharp edge of the feeding hole begins to interfere with the flow entering the bearing clearance. In fact, if this interference does not significantly alter the flow pattern of the orifice jet within the feeding hole, one would expect the pressure recovery within the feeding hole to be essentially independent of clearance for all h < 15 mils.

Values of (1 - β) measured for P_c/P_s greater than 0.95 were slightly greater than 0.74 as can be seen in Fig. 15. This apparently is connected with the fact that the supply line Reynolds number was less than 2000 for these pressure ratios.

Measurement of Overall Pressure-Flow Characteristics with Combined Orifice Restriction and Inherent Compensation

In the last phase of this study, measurements were made of bearing pressure flow characteristics under conditions where both orifice restriction and inherent compensation were important. A typical pressure profile for the bearing with orifice in

place is shown in Fig. 16. Just at the center of the orifice jet (r = 0) the pressure tap in the bottom plate senses a pressure nearly equal to the supply pressure. At positions of increasing r within the feeder hole, the pressure sensed by the pressure tap decreases rapidly until it reaches a minimum at $r \approx 0.07$. At this point the flow from the orifice begins to recover some of its dynamic pressure within the feeding hole. At $r \approx 0.09$ the flow accelerates sharply as it begins to enter the bearing film and there is an abrupt decrease in pressure down to a sharp local minimum point at r = 0.102. This minimum point corresponds to the location of the entrance vena-contracta. From $r \approx 0.102$ outward, the flow recovers some of the dynamic pressure from the entrance vena contracta and then begins to approach the theoretical viscous pressure profile in the bearing film. An enlarged plot of the pressure profile in Fig. 16 in the vicinity of the feeding hole is shown in Fig. 17.

It is instructive to compare the pressure profile shown in Fig. 16 with the pressure profile in Fig. 6, both profiles having been measured at a bearing clearance of 4 mils and at nearly the same flow rate. As one can note, the pressure depression at the entrance to the bearing film is much less severe when an orifice is present in the bearing than when one is not. This is due to the previously mentioned effect that the flow from the orifice jet seems to "flatten" out in a thin layer along the surface at the bottom of the feeding hole, making it easier for the flow to enter the bearing clearance.

In Fig. 18 is shown the pressure profile in the vicinity of the feeding hole when bearing clearance was 6 mils. One can note that there is only a slight depression in the pressure profile at the entrance to the bearing film, indicating that the flow has to accelerate only slightly upon entering the bearing film. On the basis

of this and other evidence, it was concluded that the thickness of the layer of flow from the orifice jet along the bottom surface of the feeding hole is approximately 6 mils at the periphery of the feeding hole. For bearing clearances greater than six mils, the flow from the orifice jet did not have to accelerate in entering the bearing film. On the other hand, at all clearances less than 6 mils, flow did have to accelerate when entering the film.

The fact that the presence of an orifice makes it "easier" for flow to enter the bearing clearance means that the entrance loss coefficient data presented in Fig.10 would not apply directly to the bearing with an orifice installed. The error that would be incurred by direct application of this loss coefficient data is shown in Fig. 19. Here are plotted values of calculated overall pressure drop, $P_s - P_a'$, divided by measured overall pressure drop, $P_s - P_a$, for different values of the ratio of orifice hole area to the flow area at the entrance to the bearing film. $P_s - P_a'$, the calculated overall pressure drop, was determined in the following way. First, using the measured values of $\dot{m}$ and P_s, one calculates P_c, the pressure downstream of the orifice neglecting any recovery of pressure lost across the orifice. Next one uses the recovery data of Fig. 15 to determine P_i', the stagnation pressure in the feeding hole. P_i' is given by

$$1 - \beta = \frac{P_s - P_i'}{P_s - P_c} \quad \ldots\ldots\ldots\ldots\ldots\ldots\ldots\ldots\ldots\ldots \quad (7)$$

Next, one uses the entrance loss data of Fig.10 to determine P_i, the upstream pressure for the viscous pressure profile in the bearing film. P_i would be given by

$$P_i' - P_i = K\, P_{dyn} \quad \ldots\ldots\ldots\ldots\ldots\ldots\ldots\ldots\ldots\ldots \quad (8)$$

Having determined P_i, one then uses Eq. (2) to calculate P_a', the predicted ambient pressure.

As can be seen in Fig. 19, values of overall pressure drop calculated in the manner described above are larger than measured values, due to the fact that direct use of the entrance loss coefficient data result in an overestimation of entrance loss. At large values of clearance, (small values of a/a_e) this introduces little error into the overall pressure drop because entrance loss itself is small compared with the orifice loss. At small values of clearance, entrance loss is negligible compared to the viscous pressure loss in the bearing film*. At bearing clearance around 6 mils ($a/a_e = .775$), the entrance loss is a sizable fraction of the overall pressure loss, and significant error results if the overall loss is calculated by directly applying the entrance loss data in Fig. 10.

In order to determine more accurately the inherent compensation pressure loss with an orifice present in the bearing, one can replace equation (8) by the following empirical relations.

$$P_i' - P_i = K\,(P_{dyn} - P'_{dyn}) \quad ; h \leq 6 \text{ mils} \quad \ldots\ldots\ldots\ldots \quad (9)$$

$$P_i' = P_i \quad ; h \geq 6 \text{ mils} \quad \ldots\ldots\ldots\ldots \quad (10)$$

Here P_{dyn} is the dynamic pressure at the entrance to the bearing film calculated for the existing flow rate and film clearance while P'_{dyn} is the calculated dynamic pressure that would be obtained with the existing flow rate at a film clearance of 6 mils. The accuracy with which overall pressure drop can be calculated if rela-

---

*It should be noted that even when entrance or restrictor losses are small compared with viscous film losses, the stiffness of the bearing may still depend very strongly on the magnitude of the entrance and/or restrictor losses.

tions (9) and (10) are used as shown in Fig. 20. As can be seen, agreement between prediction and measurement is within 5% of all values of a/a_e. In their present numerical form, equation (9) and (10) are valid only for the particular bearing geometry used in the present tests. However, the empirical procedure for calculating inherent compensation pressure loss defined by equations (9) and (10) may have general validity for other feeding hole geometries if one determines the appropriate value of clearance for the evaluation of P'_{dyn}.

APPLICATION OF EXPERIMENTAL RESULTS

In order to illustrate the significance and potential application of the experimental findings on feeding region pressure loss presented in this report, we shall compare the theoretical performance of a bearing as calculated on the basis of these findings with the theoretical performance of the same bearing calculated by a simplified treatment of the feeding region which has been in generally accepted use by many designers. The bearing to be analyzed is assumed to have a feeding hole geometry and orifice geometry which are directly scaled down from the feeding hole and orifice geometry of the present test bearing. The reduction factor used is four. This scaling down is done in order to consider more realistic bearing operating conditions. The geometry and the operating conditions for the bearing to be analyzed are as follows:

$R = 1$ in.

$r_i = 0.025$ in.

$a = 1.77 \times 10^{-4}$ in^2

$P_s = 37.5$ psia

$P_a = 15.0$ psia

Since the feeding hole proportions are the same as those in the test bearing, the flow pattern from the orifice to the entrance of the film of the scaled-down bearing should be the same as in the test bearing. It is assumed, therefore, that the empirical equations (9) and (10) would apply directly to the scaled-down bearing, provided P'_{dyn} is evaluated at 1.5 mils rather than at 6 mils. With this assumption, calculation of the load carrying capacity of the bearing involves the following steps: First, one guesses at a value for P_i, the stagnation pressure in the bearing film at the edge of the feeding hole. Next, one solves for Q_s, the flow rate, by

means of equation (2). Knowing Q_s (and hence $\dot{m}$) one solves equation (5) for P_c, the pressure at the vena contracta just below the orifice. P_i', the stagnation pressure in the feeding hole, is then determined from equation (7). Finally, P_i is calculated from equation (9) or (10) using the entrance loss data of Fig. 10. If this calculated value of P_i does not agree with the guessed value, then a new estimate is made for P_i and the above calculations are repeated. This trial and error procedure is repeated until the correct value for P_i is determined.

Once P_i is determined, the correct value for Q_s will be determined, and the pressure distribution in the bearing will be given by equation (1). The load carried by the bearing is obtained by integration of the pressure distribution. The general solution for the integral of the pressure distribution given by equation (1) is presented in Ref. 4.

The simplified procedure for calculating pressure loss in the feeding region of hydrostatic bearings which has been in common use involves, essentially, creating the annular restriction at the entrance to the bearing film as a variable orifice. This entrance restriction is "lumped" together with the fixed orifice in the feeding line so that one orifice equation is used to express the total pressure drop over the entire feeding region. The equation used is

$$\frac{\dot{m}}{g_c} = \alpha \sqrt{\eta} \frac{a}{\sqrt{1+\left(\frac{a}{2\pi r_i h}\right)^2}} \left\{ P_s \frac{\rho_s}{g_c} \left(\frac{P_i}{P_s}\right)^{\frac{2}{K}} \left(\frac{K}{K-1}\right) \left[1 - \left(\frac{P_i}{P_s}\right)^{\frac{K-1}{K}} \right] \right\}^{1/2} . \quad (11)$$

Note that this is identical to equation (4) except that the fixed orifice area, a, has been replaced by the term $a/\sqrt{1+(a/2\pi r_i h)^2}$. This term accounts for the fact that there are two restrictions in series, i.e. the fixed orifice and the variable inlet restriction of area $2\pi r_i h$. This simplified method of treating orifices in series is based on analysis by Heinrich (Ref. 5).

In applying equation (11) to the bearing under consideration, the values used for α and η were those measured for the fixed orifice discharging directly to atmosphere. The procedure for calculating the performance of the bearing was as follows: First, as in the case of the more detailed calculation, one guesses at the value for P_i, the stagnation pressure in the bearing film at the edge of the feeding hole. Choosing a value for P_i fixes $\dot{m}$, the mass flow rate through the bearing. One then solves Eq. (11) for P_i. If this calculated value for P_i does not agree with the guessed value, the procedure is repeated. Once the appropriate value for P_i is determined, the load carried by the bearing is obtained by integration of the pressure distribution given by Eq. (1).

Two curves of bearing load vs. clearance are shown in Fig. 21. The solid curve was calculated by the detailed method using the entrance loss data given in this present report, and the dashed curve was calculated by the simplified approach outlined above. As can be seen, the simplified analysis gives values of load consistently about 10 % to 20 % less than is calculated by the detailed analysis. This is because in the simplified analysis, pressure drop over the feeding region is overestimated. This, in turn, is due to neglect of three factors: (1) the existence of pressure recovery in the feeding hole; (2) The fact that the loss coefficient at the entrance to the bearing film is significantly less than would be predicted for an orifice of equivalent throat area and (3) the fact that the presence of a fixed orifice upstream of the film entrance will further reduce entrance losses.

Values of the stiffness of the bearing were determined from the slopes of the load vs. clearance curves in Fig. 21 and are plotted in Fig. 22. As can be seen, the stiffness characteristics of the bearing are even more strongly affected by the method used to calculate entrance losses than are the load characteristics. At low clearances, there exists a difference of as much as 2 to 1 between the stiffness based on the detailed method of calculating feeding region pressure loss and the

stiffness based on the simplified loss calculations.

The predicted flow rate also depends significantly on the method of calculating feeding region loss. In the case of a double acting bearing, where clearance is set by machining, the percentage error in the predicted flow would be approximately the same as the percentage error in the predicted load. For a single-acting thrust bearing, however, the operating clearance depends on the load. Since flow rate is roughly proportional to clearance to the third power, a relatively small error in predicting the load vs. clearance relationship for a single-acting thrust bearing can result in a considerable error in the predicted flow rate for a given load. For example, a bearing designed on the basis of the simplified calculation curve in Fig. 21 to carry a load of 9.05 lbs at h = 0.98 mils would have a predicted flow rate of 0.919×10^{-4} lbs/sec. In actuality, according to the detailed calculations, a load of 9.05 lbs would be carried at a clearance of 1.15 mils with a corresponding flow rate of 1.55×10^{-4} lb/sec.

The results of the comparison between the simplified method of treating restriction with the detailed calculations can be summarized as follows. Compared with the predicted performance based on the simplified approach, the detailed calculations showed that:

1. A higher load would be carried with the same gap.
2. The maximum stiffness would be realized at a larger gap, and the magnitude of the maximum stiffness would be somewhat smaller. For a double-acting thrust bearing designed according to the simplified calculations for maximum stiffness, the realized stiffness would be lower by 20 %.
3. For a double-acting thrust bearing, the realized flow rate would be somewhat higher in nearly the same proportion as the realized load is higher. For a single-acting thrust bearing designed for a given load, the realized operating clearance would be slightly larger while the flow rate would be as much as 70 % higher.

SUMMARY AND CONCLUSIONS

Measurements were made of the film entrance loss or inherent compensation loss for sharp-edged feeding holes. These data were expressed in terms of a loss coefficient, K, multiplying the dynamic pressure at the entrance to the bearing film. This loss coefficient was found to be a function of the Reynolds number at the entrance to the bearing film. Other dimensionless parameters which could influence this loss coefficient are the film entrance Mach number and the geometrical ratio h/r_i. In the present tests, values of entrance Mach number were always less than 0.4. In this range no significant dependence of K on Mach number was observed.

Concerning the dependence of K on h/r_i, it can be argued that if this geometrical ratio is sufficiently small, it should not significantly affect the film entrance loss. The measured pressure profiles indicate that entrance loss is associated with the development of a vena contracta at the film entrance, the entrance loss presumably being caused by the formation of eddies in the sharply diverging flow downstream of the vena contracta. The length required for the flow downstream of the vena contracta to fill the bearing clearance and for eddying to die out should be proportional to h, the equivalent hydraulic radius of the film. If h is small compared with r_i, then the amount of radial divergence of the bearing film that takes place over the length required for the flow to "recover" downstream of the vena contracta will be negligible and should have negligible effect on the vena contracta loss. Conversely, if h/r_i is sufficiently large, then significant radial divergence of the bearing film will occur over the recovery length, and this divergence would act to increase the entrance loss.

In the present tests, with $h/r_i \leq 8 \times 10^{-2}$, K appeared to be independent of h/r_i. We may therefore conclude that the single curve of K versus Re' shown in Fig. 10 is generally valid for sharp edged feeding holes with no orifice present under the conditions $h/r_i \leq 8.0 \times 10^{-2}$ and Mach number less than 0.4. Comparison with data taken at Franklin Research Institute supports this conclusion. The fact that Franklin data taken at $h/r_i = 16 \times 10^{-2}$ yielded loss coefficients significantly higher than those measured at lower values of h/r_i may be evidence of the beginning influence of radial divergence on entrance loss. It is also possible, however, that these higher loss coefficients were the result of weak shock phenomena in the bearing film.

It was found that a significant fraction of the dynamic pressure from an orifice jet was recovered within the feeding hole of a hydrostatic bearing when the jet impinged on the bearing surface at the bottom of the feeding hole. Since the depth of the feeding hole was large compared with the bearing clearance, changes in clearance had a negligible effect on the amount of pressure recovered. The fraction of the pressure recovered was approximately independent of the pressure ratio across the orifice, provided the Reynolds number in the supply line was greater than 2,000. In the present tests, only one feeding hole - orifice geometry was studied. The dependence of orifice pressure recovery on feeding hole geometry is an important area for future study.

Measurements of pressure profiles and overall pressure loss made under conditions where both inherent compensation restriction and orifice restriction are important showed that there is a complex relation between orifice pressure loss and bearing

film entrance loss. It was found that the presence of the orifice in the test bearing reduced the pressure loss associated with entrance of the flow into the bearing film. This reduction in entrance loss was apparently caused by the fact that flow from the orifice jet spread out in a thin, high velocity layer along the bearing surface at the bottom of the feeding hole, thus making it "easier" for the flow to enter the thin bearing clearance. Pressure profile measurements indicated that the thickness of this "layer" of flow from the orifice was approximately 6 mils at the edge of the feeding hole. For clearances greater than 6 mils, there was no film entrance loss when an orifice was present in the bearing. Based on the finding, a modified procedure for calculating entrance pressure loss with orifice present was presented which made use of the entrance loss coefficients measured for the case of no orifice present. This modified procedure enabled one to calculate overall bearing pressure loss to within five percent accuracy.

The relationship between the flow restriction at the entrance to the bearing film and the flow restriction of the orifice is like the relationship between two orifices in series. If the second orifice were to have a hole which was slightly larger than that of the first orifice, and if the orifices were close together, then the high velocity jet from the first orifice might be able to pass straight through the second orifice hole with little or no obstruction. In this case, one would overestimate the pressure drop across both orifices by computing the pressure loss over each orifice separately, and adding them. This is essentially the situation to which Fig. 19 applies. One can note that the maximum overestimation of overall bearing pressure loss in this figure occurs at $a/a_e = 0.775$, i.e. when the film entrance area is about 30% greater than the orifice area.

The relation between the orifice restriction and the pressure loss at the entrance to the bearing film will depend on the geometry of the feeding hole. Therefore, the particular empirical equations (Eq. 9 and 10) used to calculate entrance loss in this report are probably not valid for other geometries. It is possible, however, that these empirical equations could be generalized to be applicable to other feeder hole dimensions. The adoption of equations (9) and (10) was based, essentially, on the observation that the thickness of the layer of flow from the orifice was approximately 6 mils at the edge of the feeding hole. To generalize equations (9) and (10) it would be necessary to determine the effective thickness of this layer of flow at the edge of feeding holes of various sizes and shapes. Perhaps this effective thickness could be determined analytically, by consideration of the problem of the flow of a jet against a flat plate. In any case, whether determined analytically or empirically, the effective thickness of the layer of flow from the orifice should be able to be determined as a function of dimensionless parameters such as the ratio of feeding hole depth to feeding hole radius and the ratio of orifice radius to feeding hole radius. Thus, in the generalized form of equations (9) and (10), the specific condition that P'_{dyn} be evaluated at 6 mil clearance could, perhaps, be replaced by a more general criteria in which the thickness at which to evaluate P'_{dyn} would be expressed non-dimensionally as a function of various pertinent parameters.

NOMENCLATURE

a	Orifice flow area, in^2.
a_e	Flow cross section area at entrance to bearing film = $2\pi r_i h$, in^2.
a^*	Flow cross section area for flow to attain sonic speed (M=1) by isentropic acceleration from stagnation conditions in feeding hole, in^2.
c	Speed of sound, in/sec.
c^*	Speed of sound at M = 1, in/sec.
d	Inner diameter of supply line, in.
g_c	Gravitational constant = 386 in^2/sec.
h	Bearing film clearance, in.
K	Bearing film entrance loss coefficient.
K_o	Vena contracta coefficient for incompressible flow.
k	Ratio of specific heats.
M	Mach number = V_m/c.
M^*	Mach number based on speed of sound at M = 1, $M^* = M_m/v^*$.
$\dot{m}$	Mass flow rate lb/sec.
P	Pressure, lb/in^2.
P_a	Ambient pressure, lb/in^2.
P_c	Static pressure at vena contracta downstream of orifice, lb/in^2.
P_{dyn}	Dynamic pressure in bearing film, at film entrance, lb/in^2.
P'_{dyn}	Dynamic pressure in bearing film at film entrance assuming a bearing clearance of 6 mils, lb/in^2.
P_i	Theoretical stagnation pressure at edge of feeding hole calculated from Equation (1), lb/in^2.
P_i'	Actual stagnation pressure in feeding hole, lb/in^2.
Q	Volume flow rate, in^3/sec.
R	Outer radius of bearing, in.

Re	Reynolds number in bearing film at entrance to film.
R_e'	Reynolds number for flow in supply line for test bearing = $4\dot{m}/\pi d$.
r	Radial coordinate measured from center of bearing.
r_i	Radius of feeding hole, in.
V	Flow velocity, in/sec.
V_m	Mean flow velocity, in/sec.
α	Vena contracta coefficient.
β	Orifice recovery factor
η	Orifice "efficiency" coefficient
μ	Fluid viscosity, $\frac{\text{lb-sec}}{\text{in}^2}$
ρ	Fluid density, lb/in^3.

Subscripts

e	Denotes conditions in bearing film at entrance to bearing film.
s	Denotes supply conditions.

REFERENCES

1. Carothers, P.F. "An Experimental Investigation of the Pressure Distribution of Air in Radial Flow in Thin Films between Parallel Plates," Master's Thesis, United States Naval Postgraduate School, Monterey, California, 1961.

2. Carfagno, S.P. and McCabe, J.T., "Summary of Investigations of Entrance Effects in Circular Thrust Bearings," Franklin Institute Research Laboratories Interim Report 1-A2049-24, 1965.

3. Pinkus, O, and Sternlicht, B., "Theory of Hydrodynamic Lubrication," McGraw Hill Book Co., 1961.

4. Licht, L., "Axial, Relative Motion of a Circular Step Bearing," Journal of Basic Engineering, Trans. ASME, Series D Vol. 81, 1959, pp. 109-117.

5. Heinrich, G., "The Theory of the Externally Pressurized Bearing with Compressible Lubricant," Proceeding of the First International Symposium on Gas-Lubricated Bearings, ONR/ACR-49, October, 1959, pp. 251-265.

6. Keenan, J. and Kaye, J., "Gas Tables," John Wiley and Sons Inc., 1948.

APPENDIX A

Calculation of P_{dyn}, the Dynamic Pressure at the Entrance to the Bearing Film

Let

$\dot{m}$ = Mass flow rate,

V_m = Mean flow velocity,

c = Speed of sound,

c^* = Speed of sound at M = 1,

a^* = Flow across section area for flow to attain sonic speed (m=1) by isentropic acceleration from stagnation conditions in feeding hole.

a_e = Flow cross section area at entrance to bearing film = $2\pi r_i h$.

M = Mach number = $\frac{V_m}{c}$.

M^* = Mach number based on speed of sound at M = 1; $m^* = V_m/c^*$.

ρ = Fluid density,

P = Pressure.

Subscripts

ρ = Stagnation conditions in feeding hole,

e = Condition in bearing film at entrance to film,

s = Supply conditions.

We have

$$\dot{m} = \rho_e (V_m)_e a_e = \frac{\rho_e}{\rho_o} c^* M_e^* a_e \rho_o \quad \ldots\ldots\ldots\ldots\ldots\ldots \quad (A.1)$$

For any test run, the quantities $\dot{m}, a_e$ and ρ_o are known. The quantities ρ_e/ρ_o and M_e^* are functions of film entrance Mach number M_e and are tabulated in the Gas Tables compiled by Keenan and Kayes (Ref. 6). Thus, we can write

$$\rho_e/\rho_o \, M_e^* = \dot{m} / c^* a_e \rho_o = F(M_e) \quad \ldots\ldots\ldots\ldots\ldots\ldots \quad (A.2)$$

where $F(M_e)$ denotes a function of M_e. From equation (A.2), knowing $\dot{m}/c^* a_e \rho_o$, one can determine M_e from the above mentioned Gas Tables. Knowing M_e, one can determine P_e/P_o, also from the Gas Tables. P_{dyn}, the dynamic pressure at the entrance to the bearing film, is then calculated as

$$P_{dyn} = P_o - P_e \quad \ldots\ldots\ldots\ldots\ldots\ldots\ldots\ldots\ldots\ldots \quad (A.3)$$

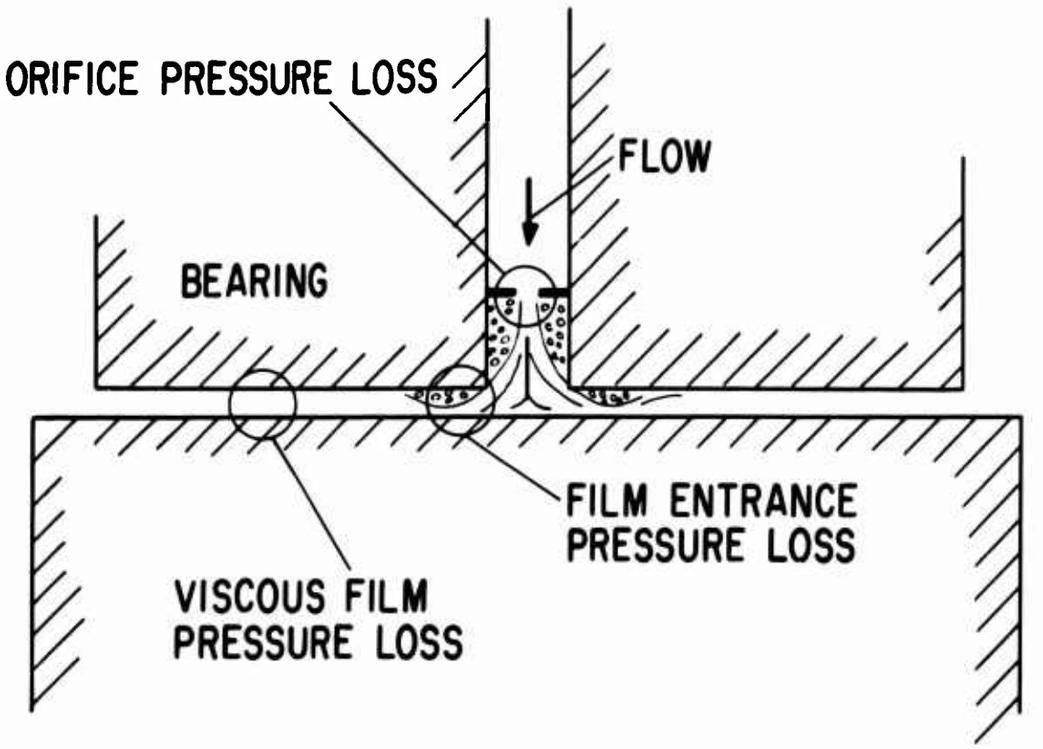

Fig. 1 Schematic Drawing of Sources of Pressure Loss in Externally Pressurized Bearing

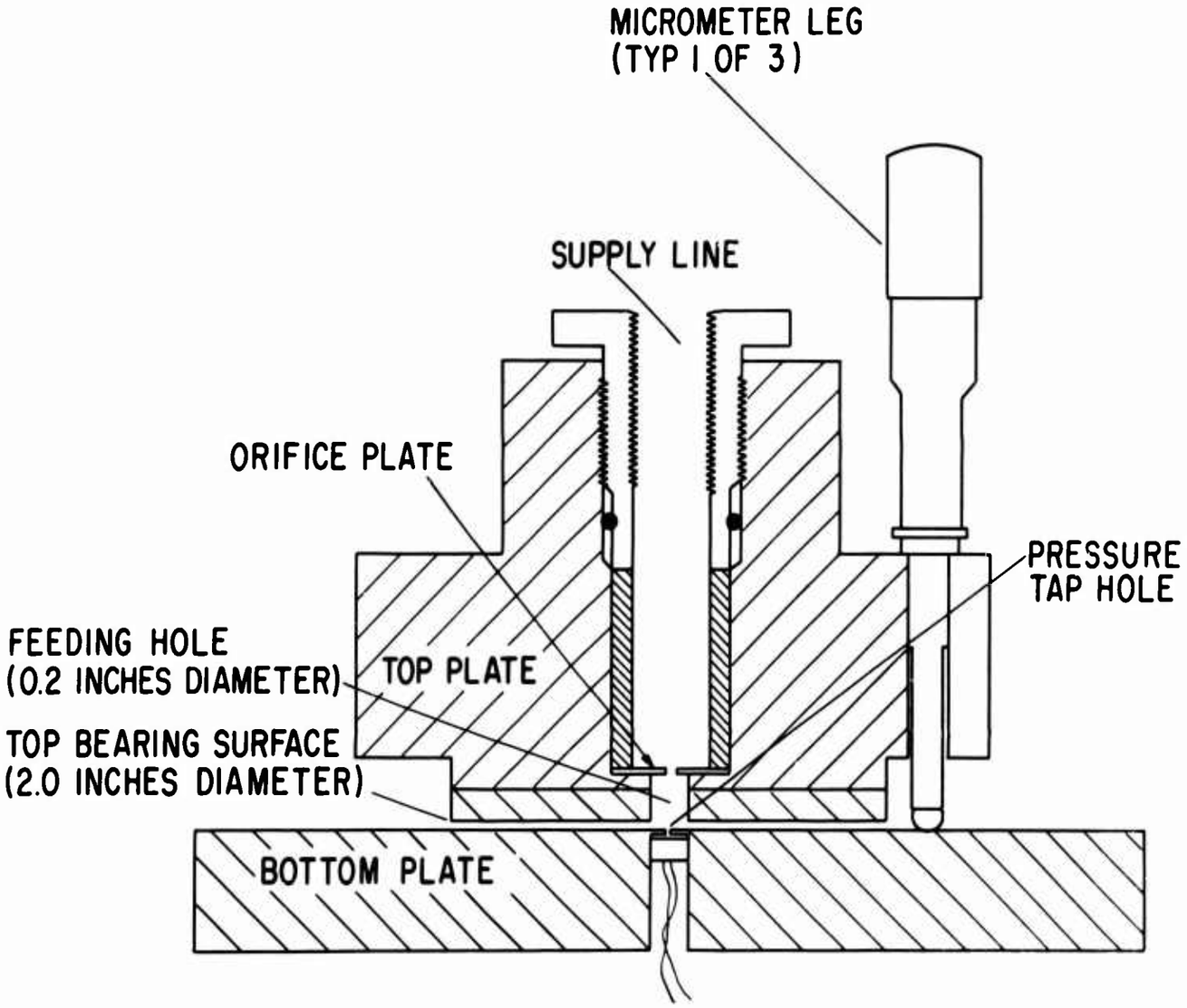

Fig. 2 Schematic Drawing of Test Bearing

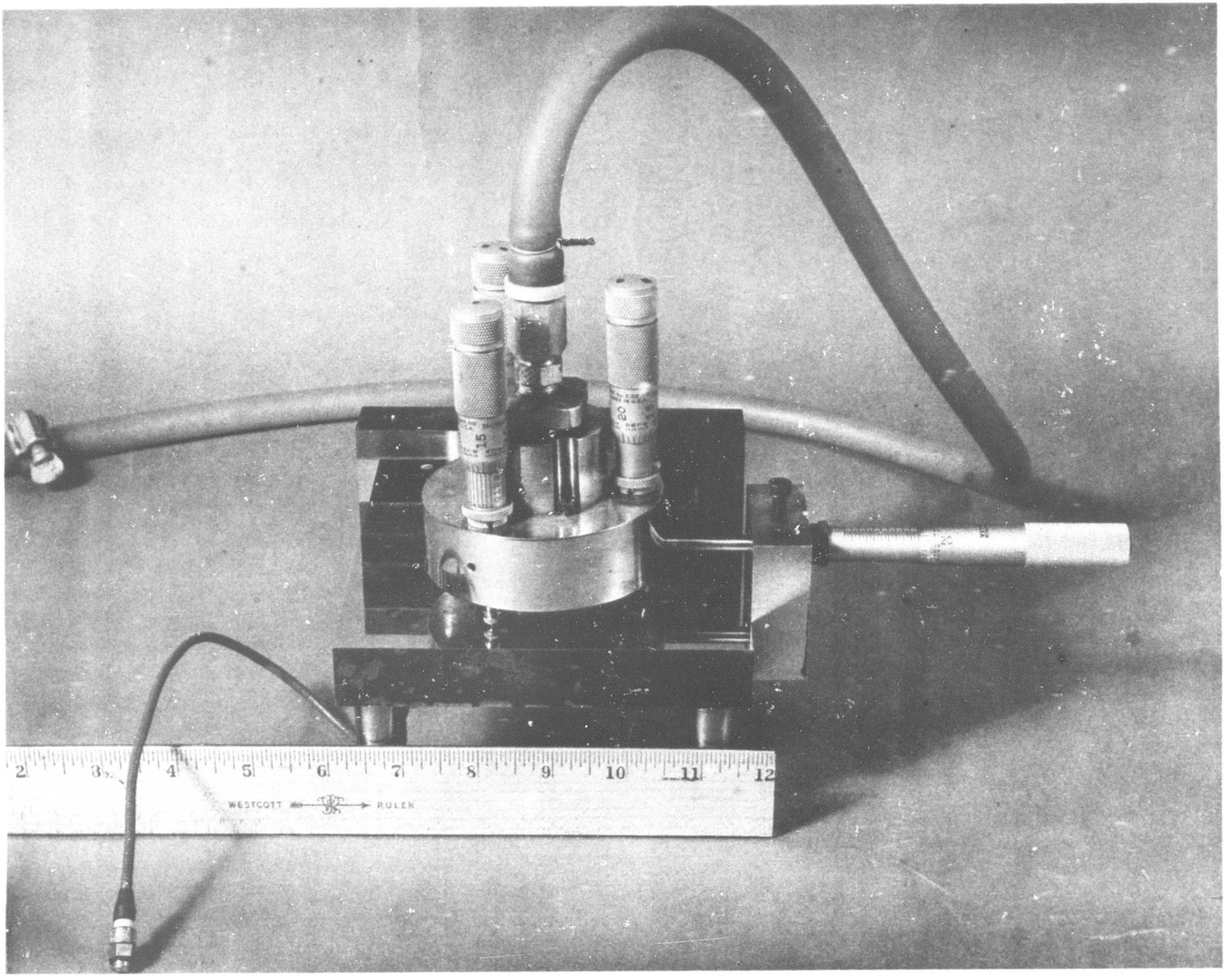

Fig. 3 Test Bearing

MTI-1376

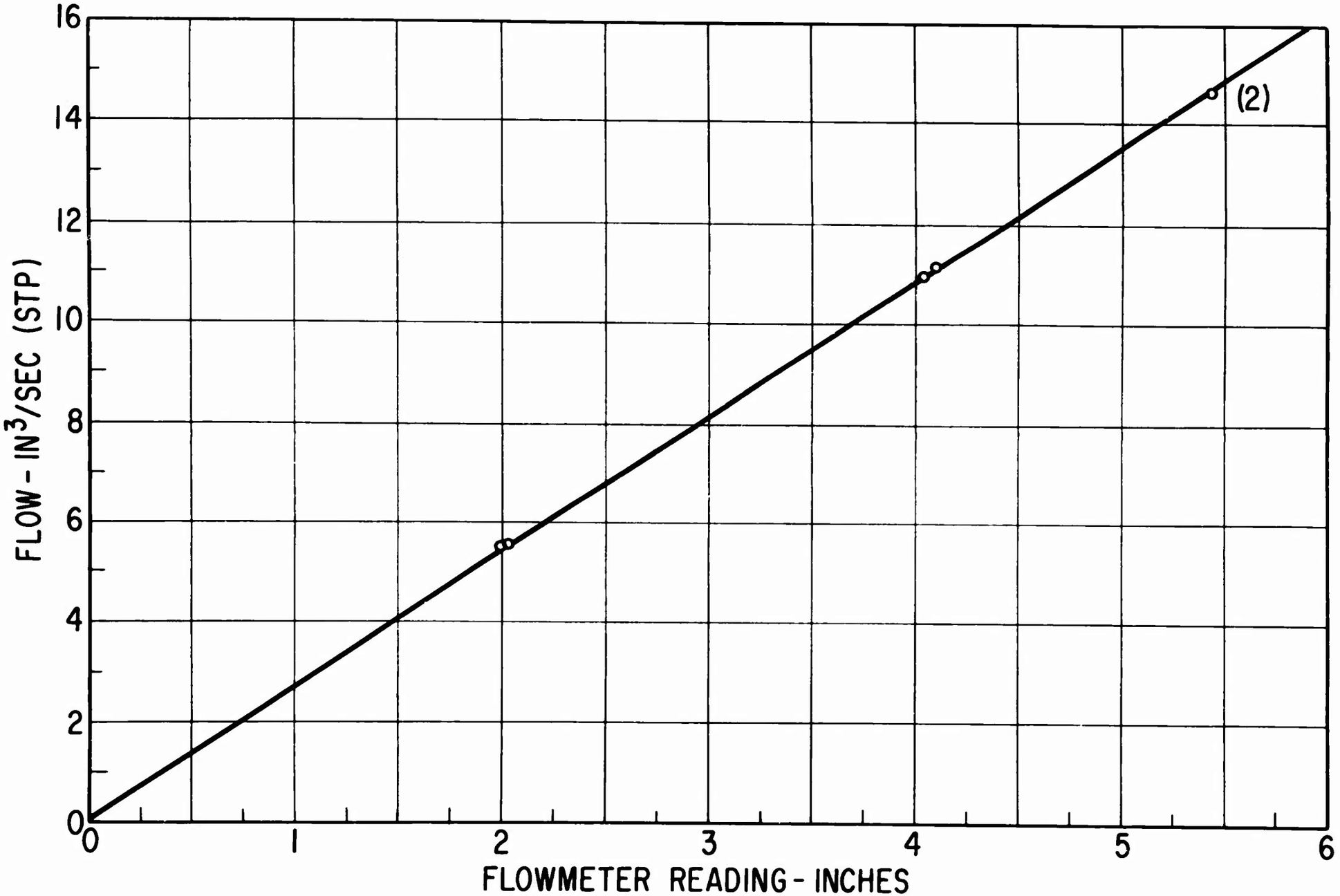

Fig. 4 Flowmeter Calibration

MTI-1377

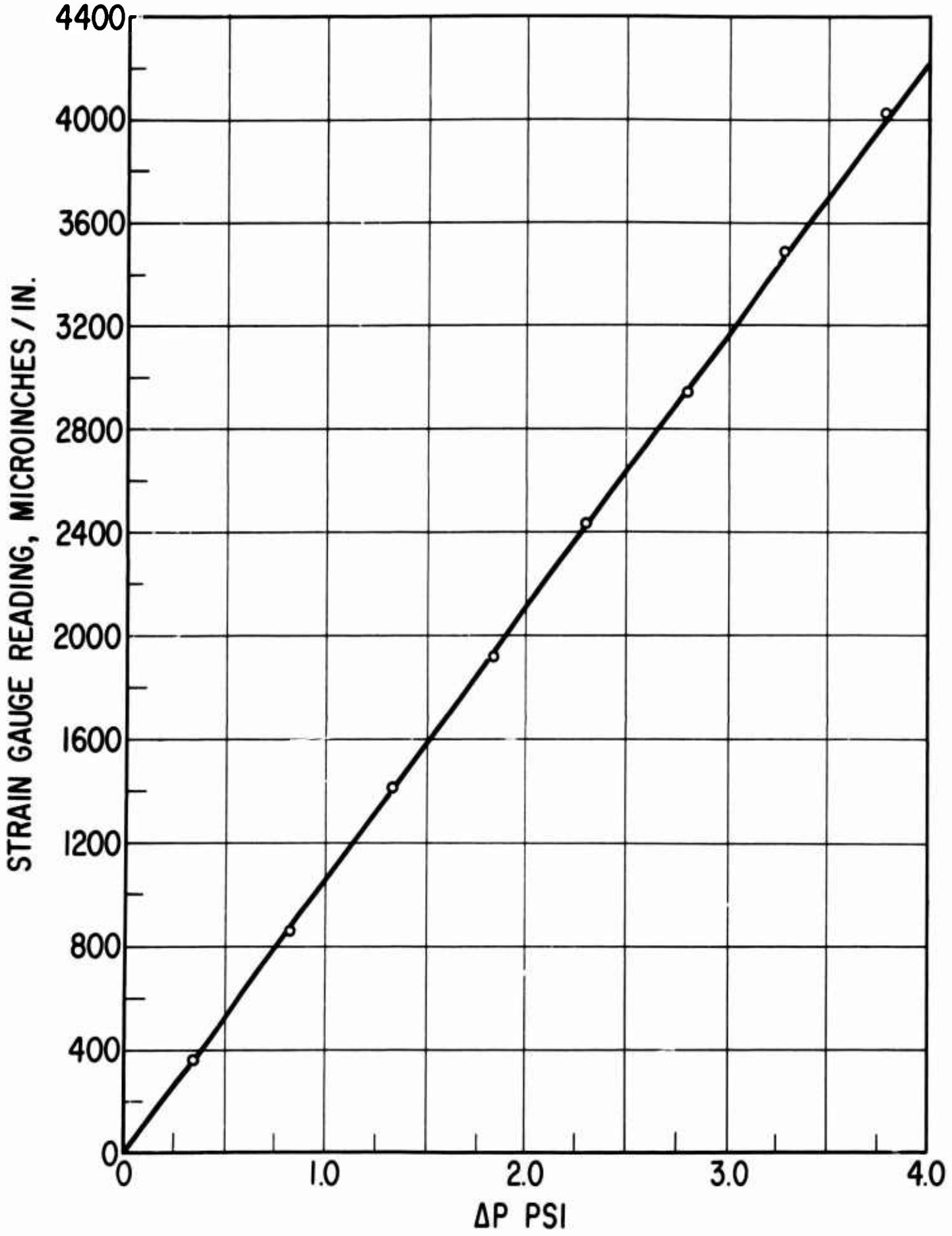

Fig. 5 Calibration Curve for Pressure Transducer

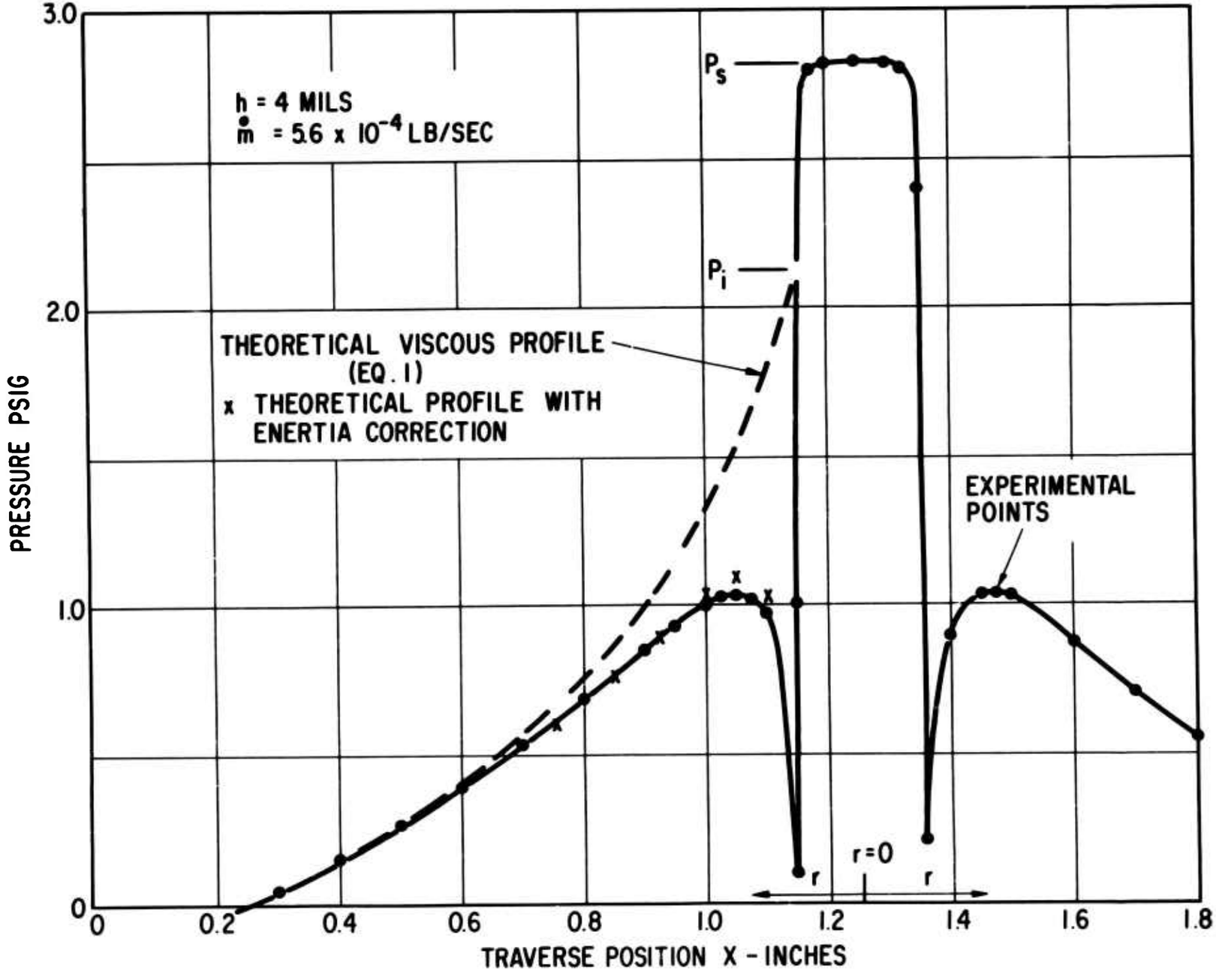

Fig. 6 Pressure Profile without Orifice

MTI-1379

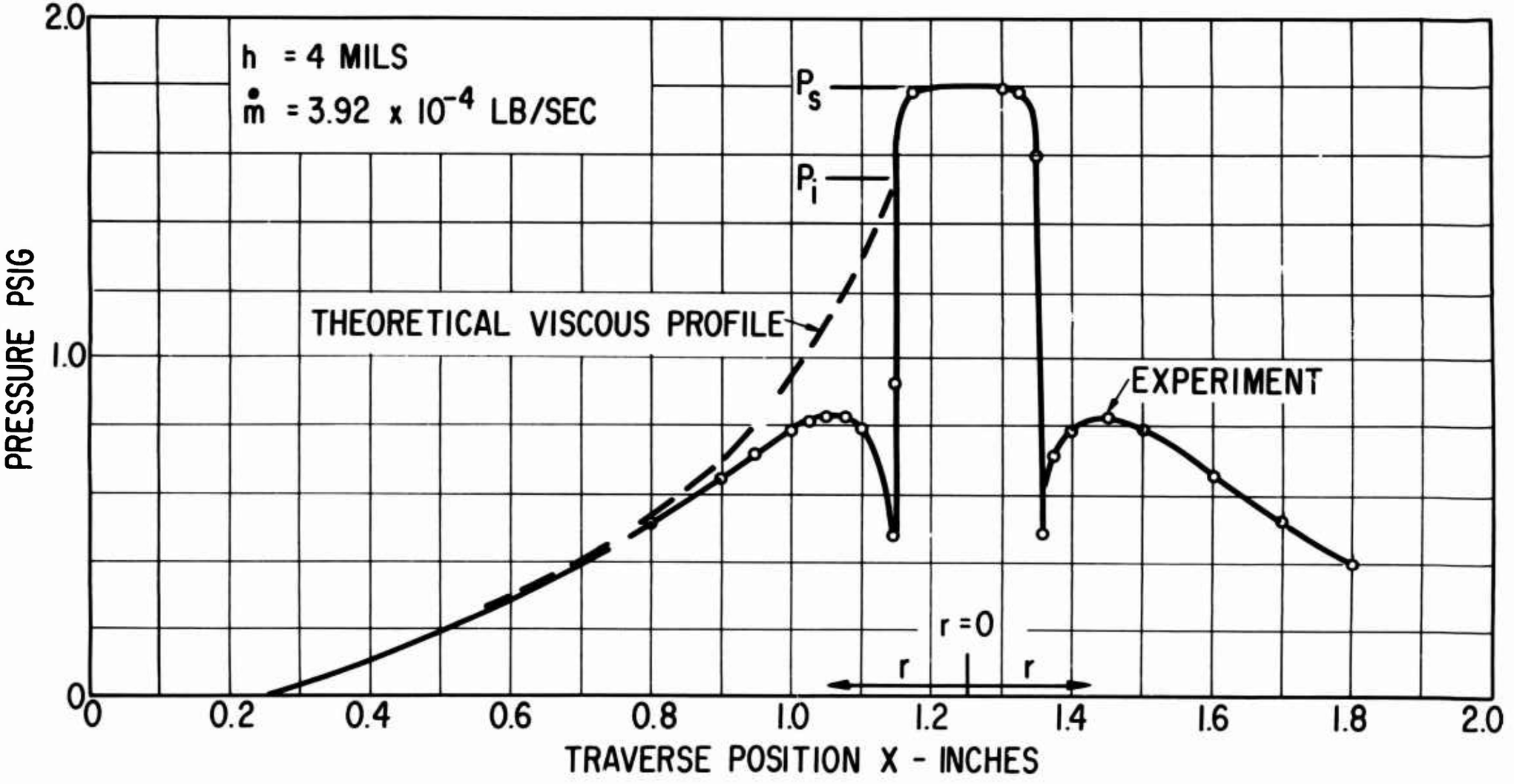

Fig. 7 Pressure Profile without Orifice

MTI-1382

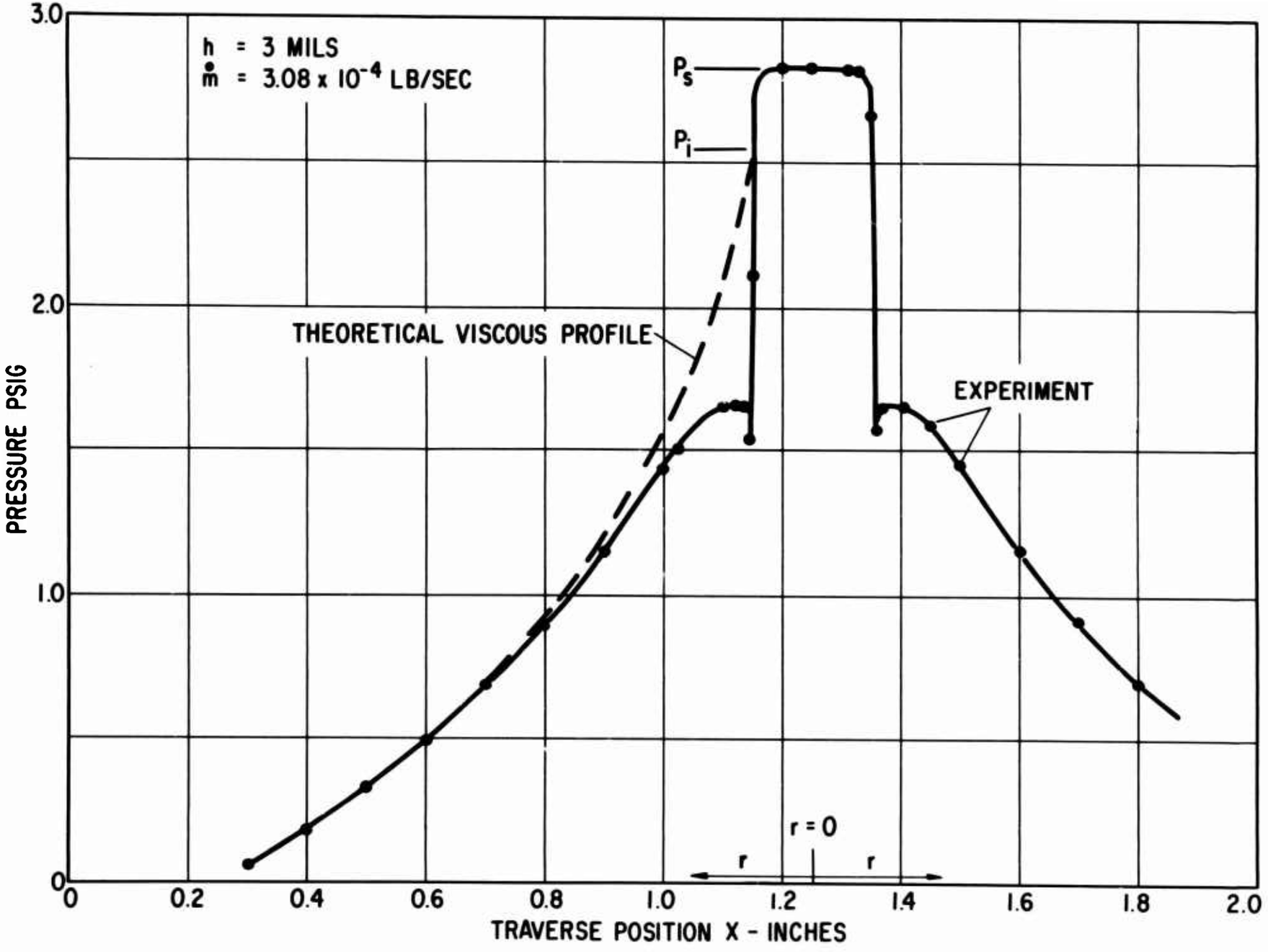

Fig. 8 Pressure Profile without Orifice

MTI-1381

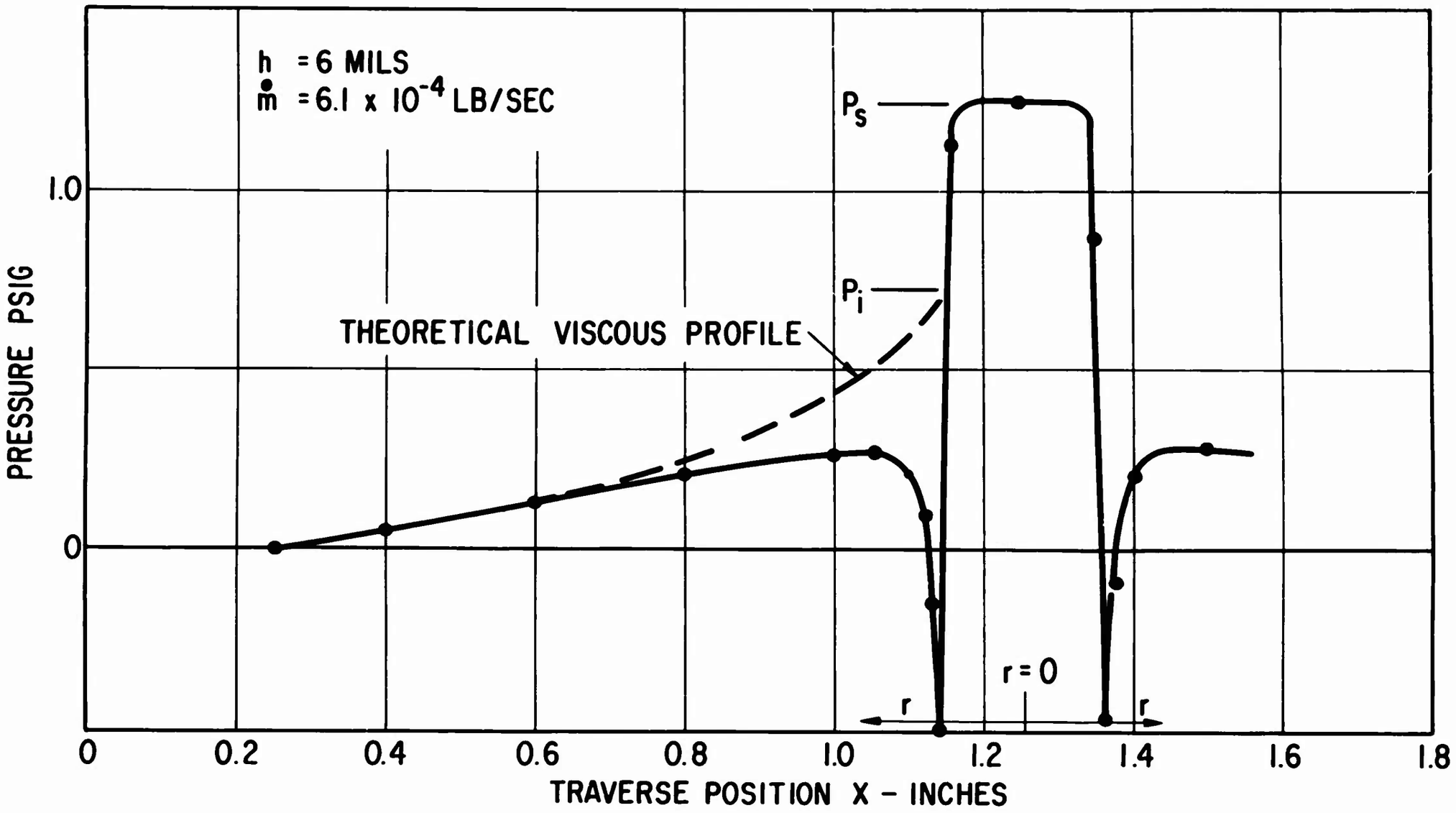

Fig. 9 Pressure Profile without Orifice

MTI-1380

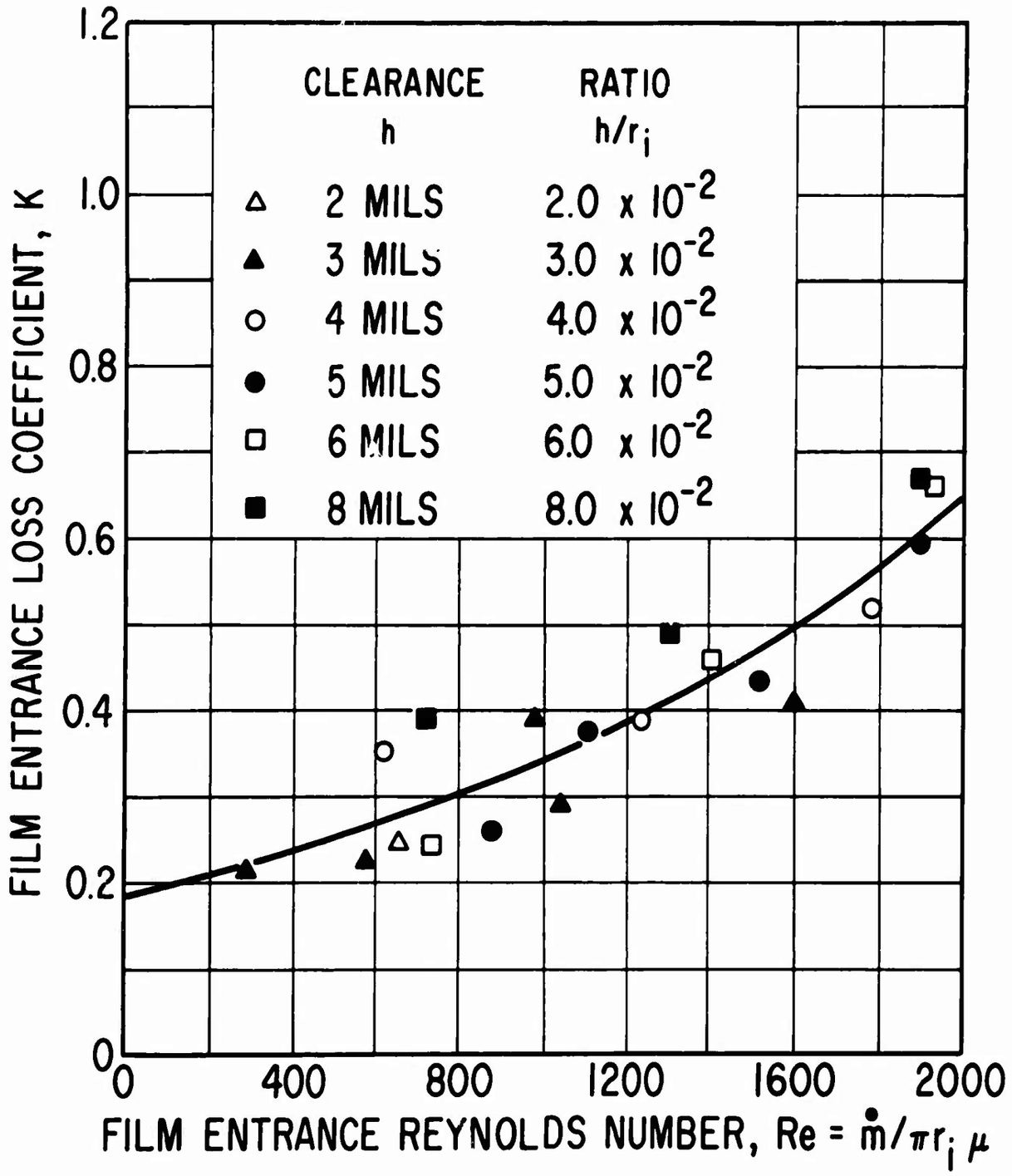

Fig. 10 Film Entrance Loss Coefficients

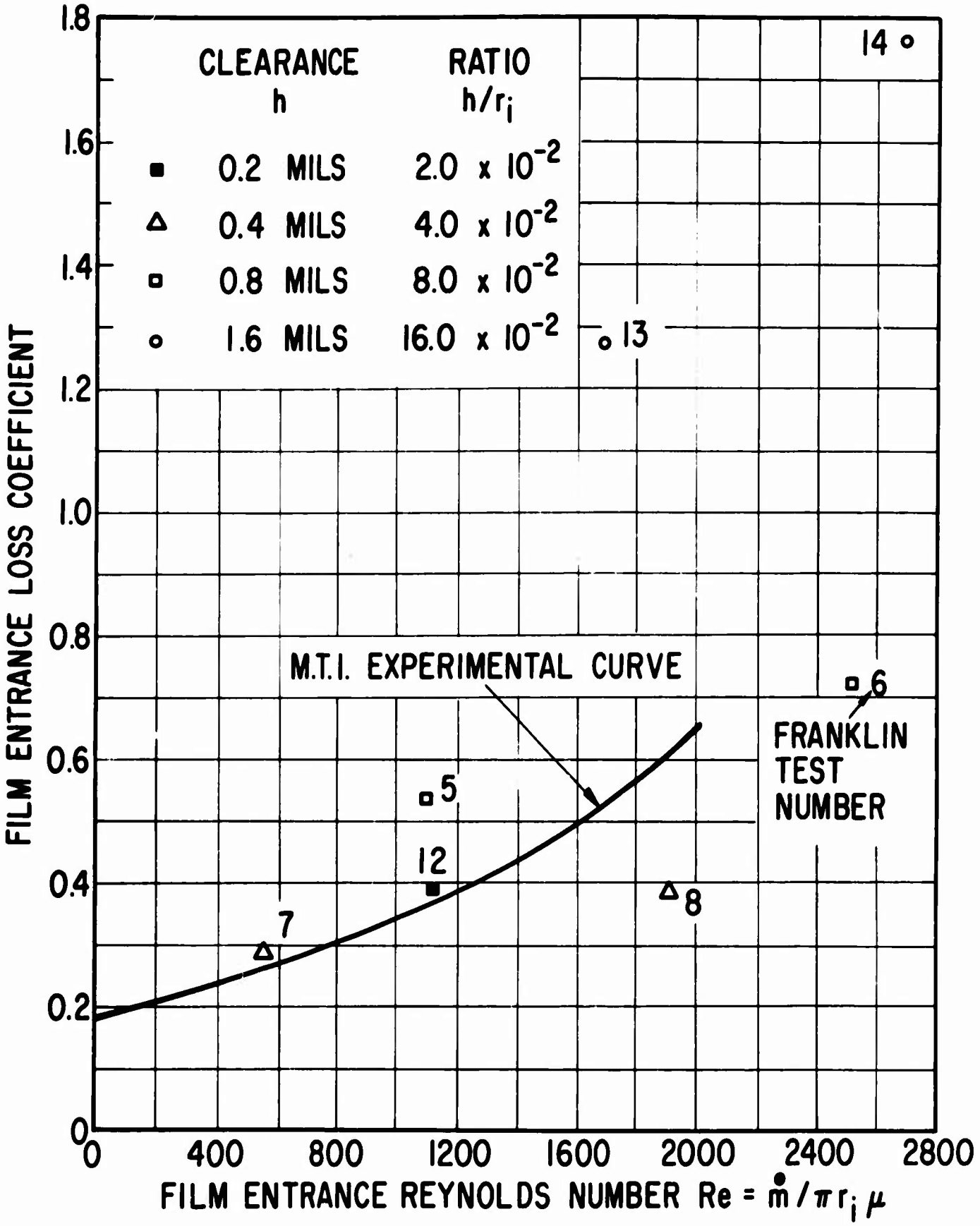

Fig. 11 Comparison with Data of Franklin Institute

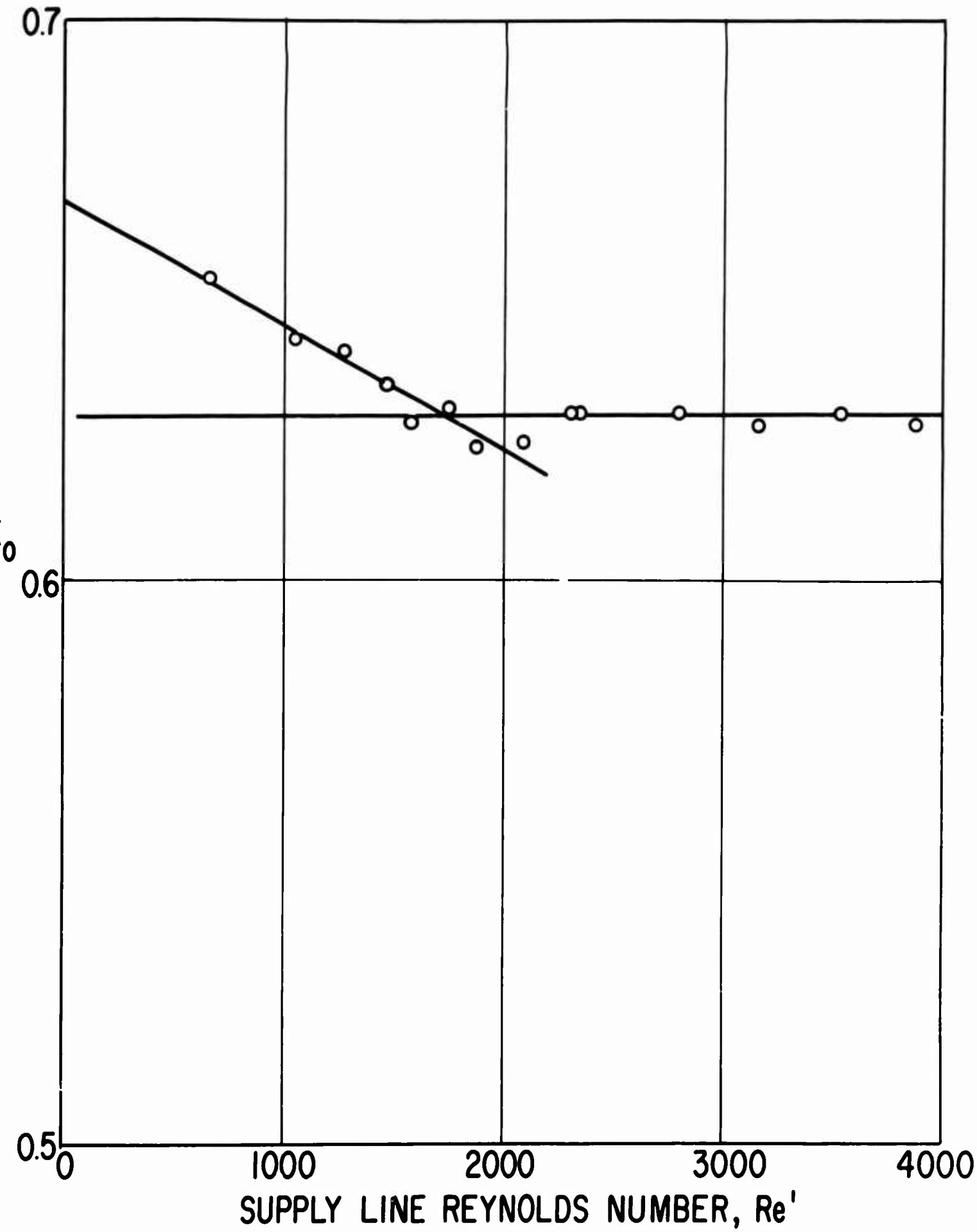

Fig. 12 Orifice Coefficient vs. Supply Line Reynolds No.

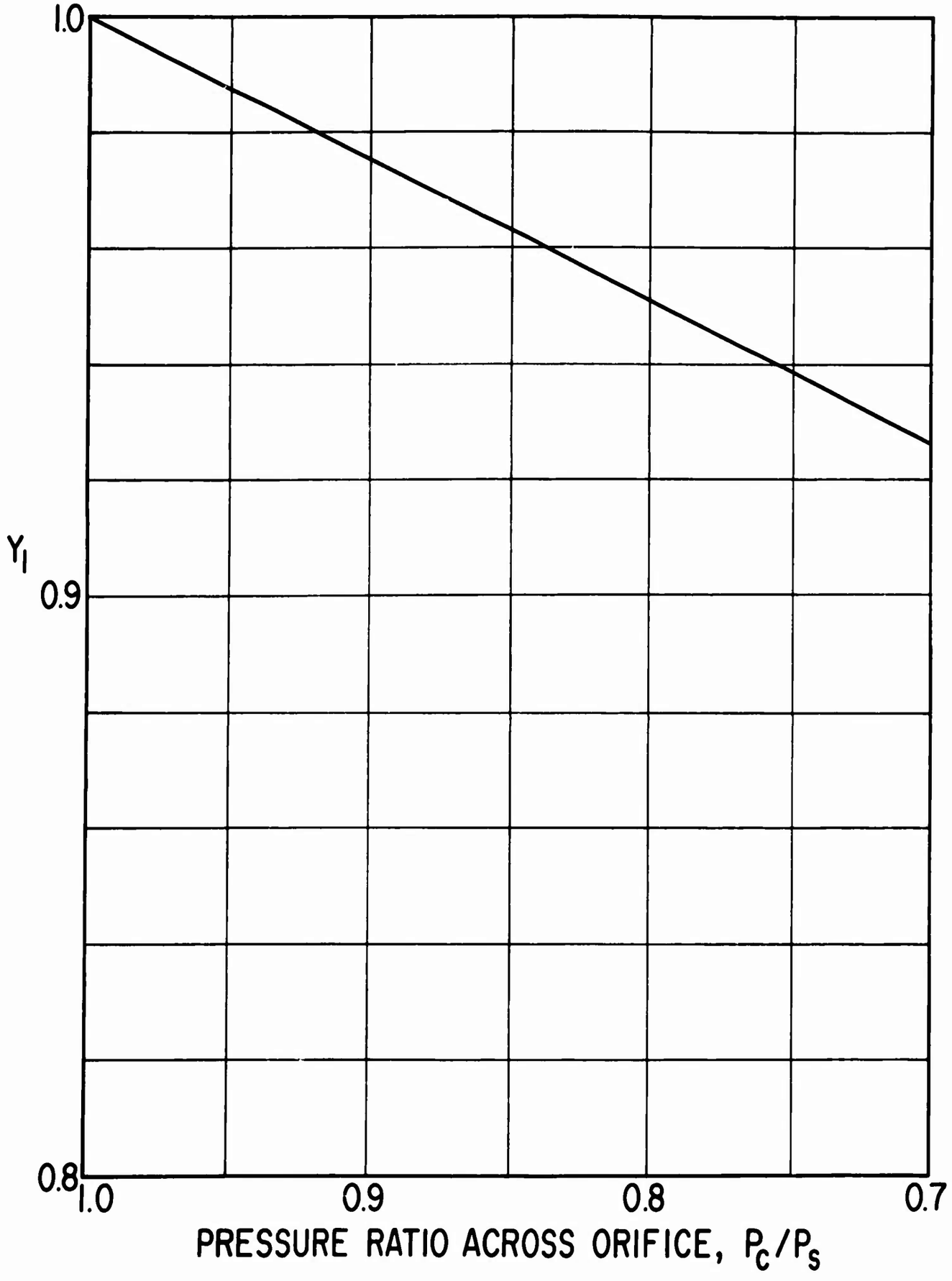

Fig. 13 Orifice Expansion Factor Y_1 vs. Pressure Ratio

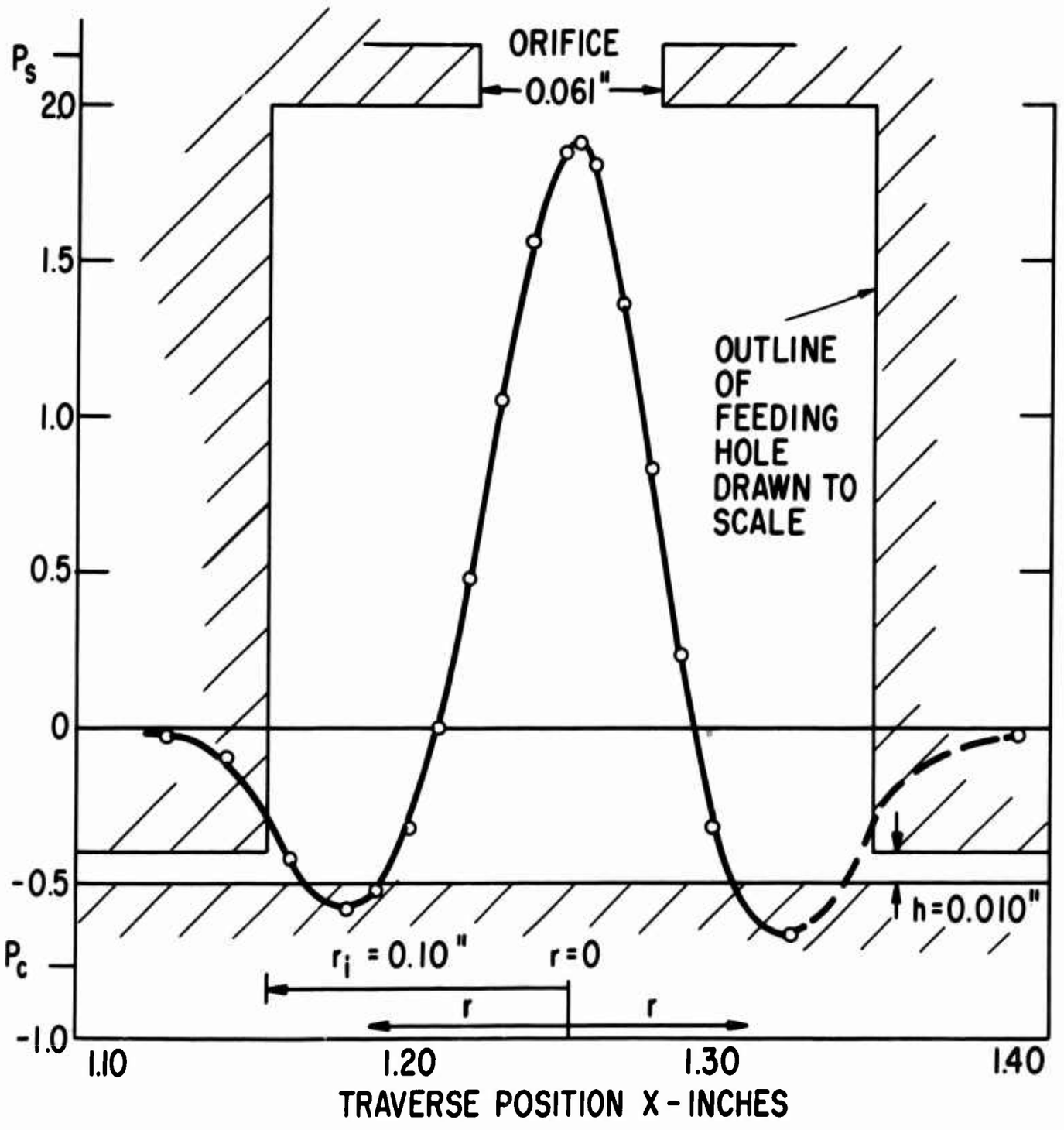

Fig. 14 Pressure Profile Across Feeding Hole with Orifice

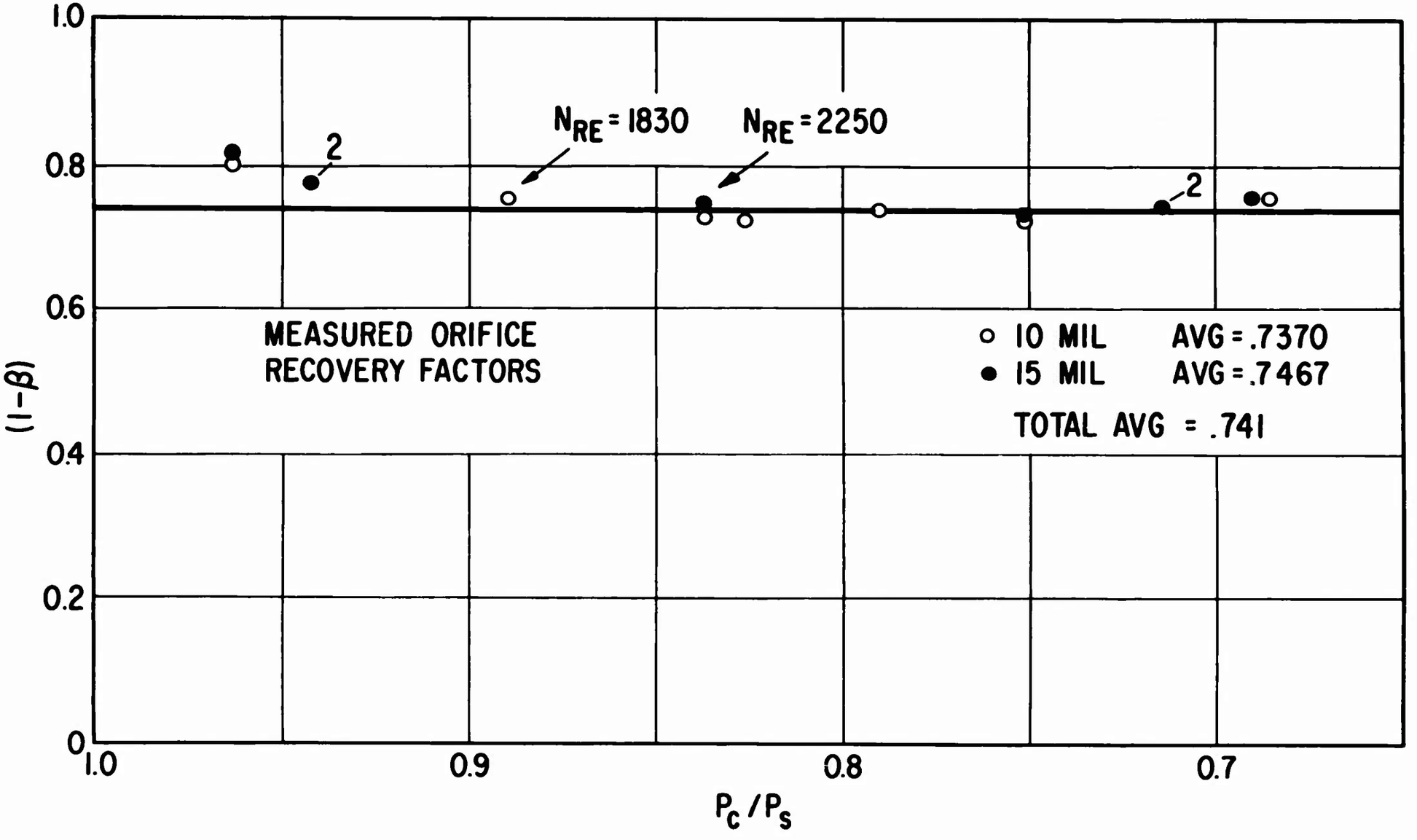

Fig. 15 Measured Orifice Recovery Factors

MTI-1388

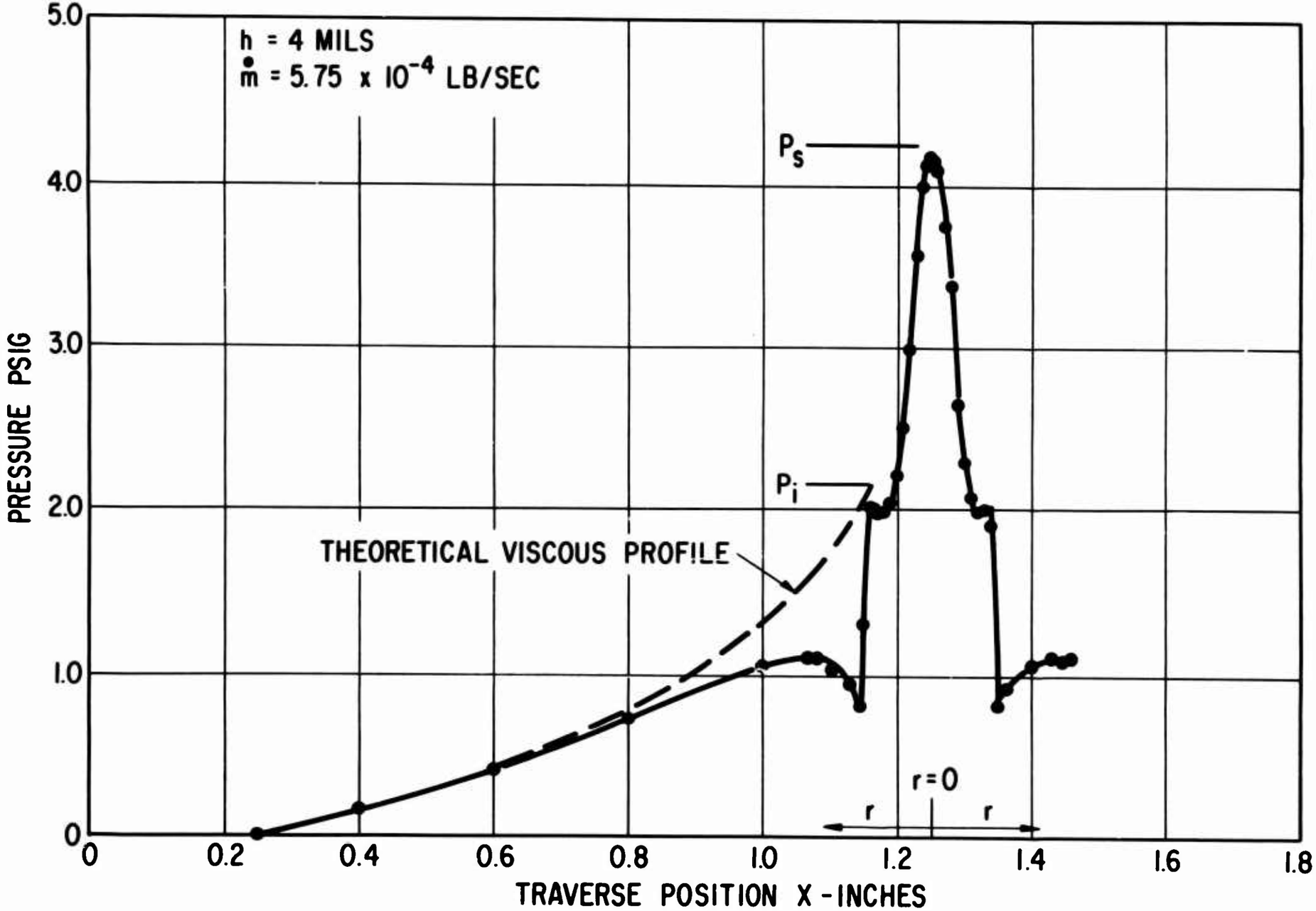

Fig. 16 Pressure Profile with Orifice Present

MTI-1389

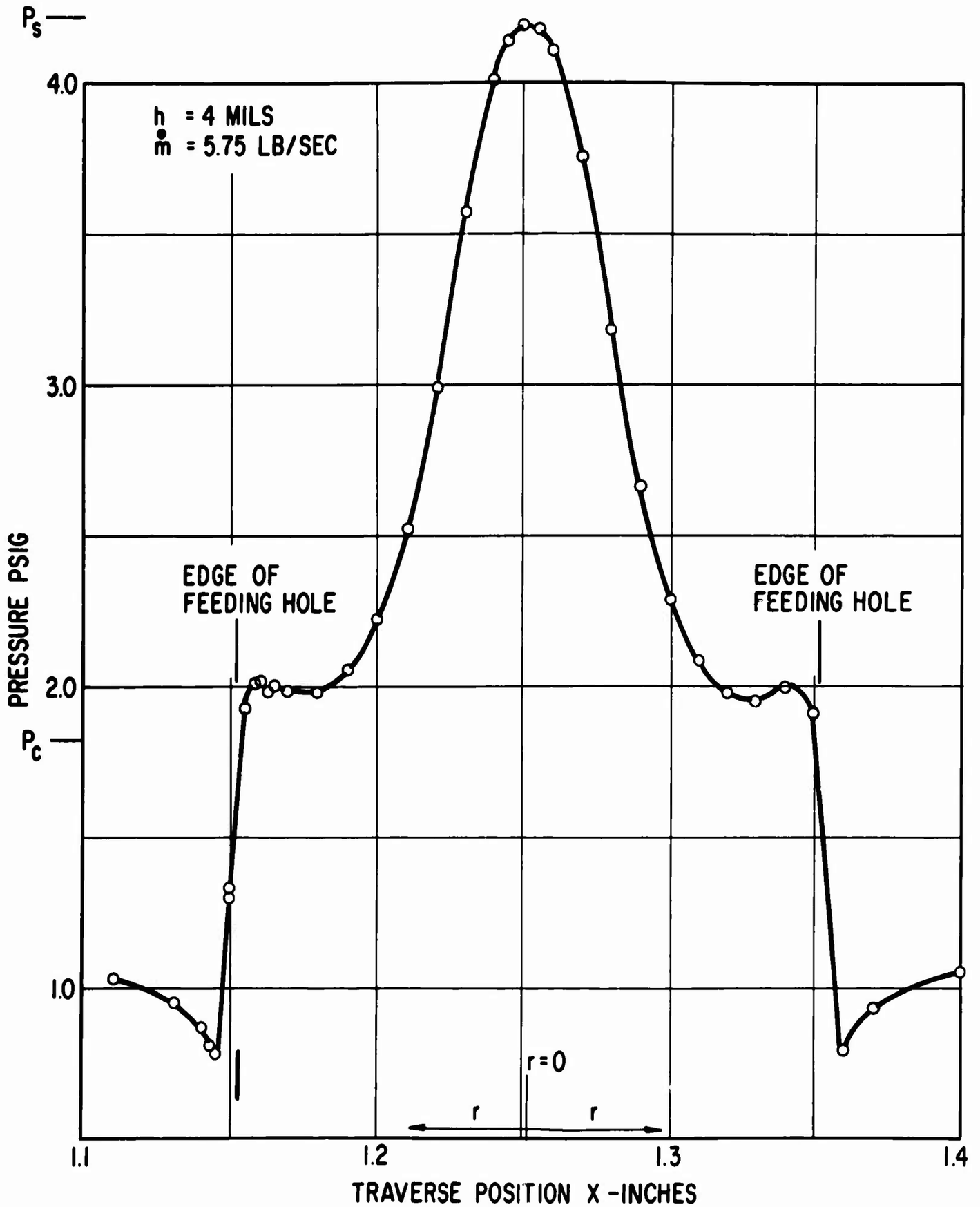

Fig. 17 Enlarged Section of Pressure Profile Shown in Fig. 16

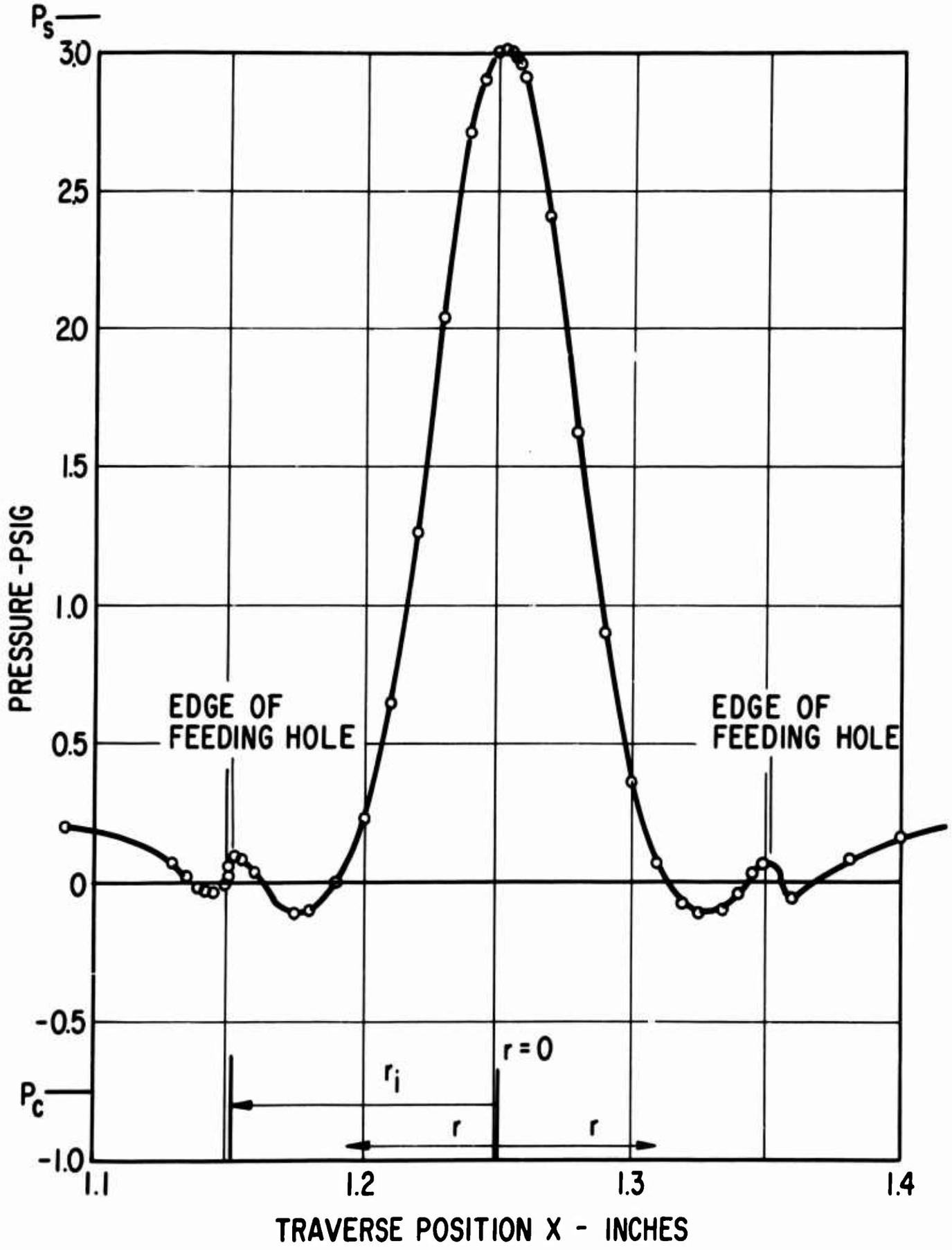

Fig. 18 Pressure Profile Across Feeding Hole with Orifice

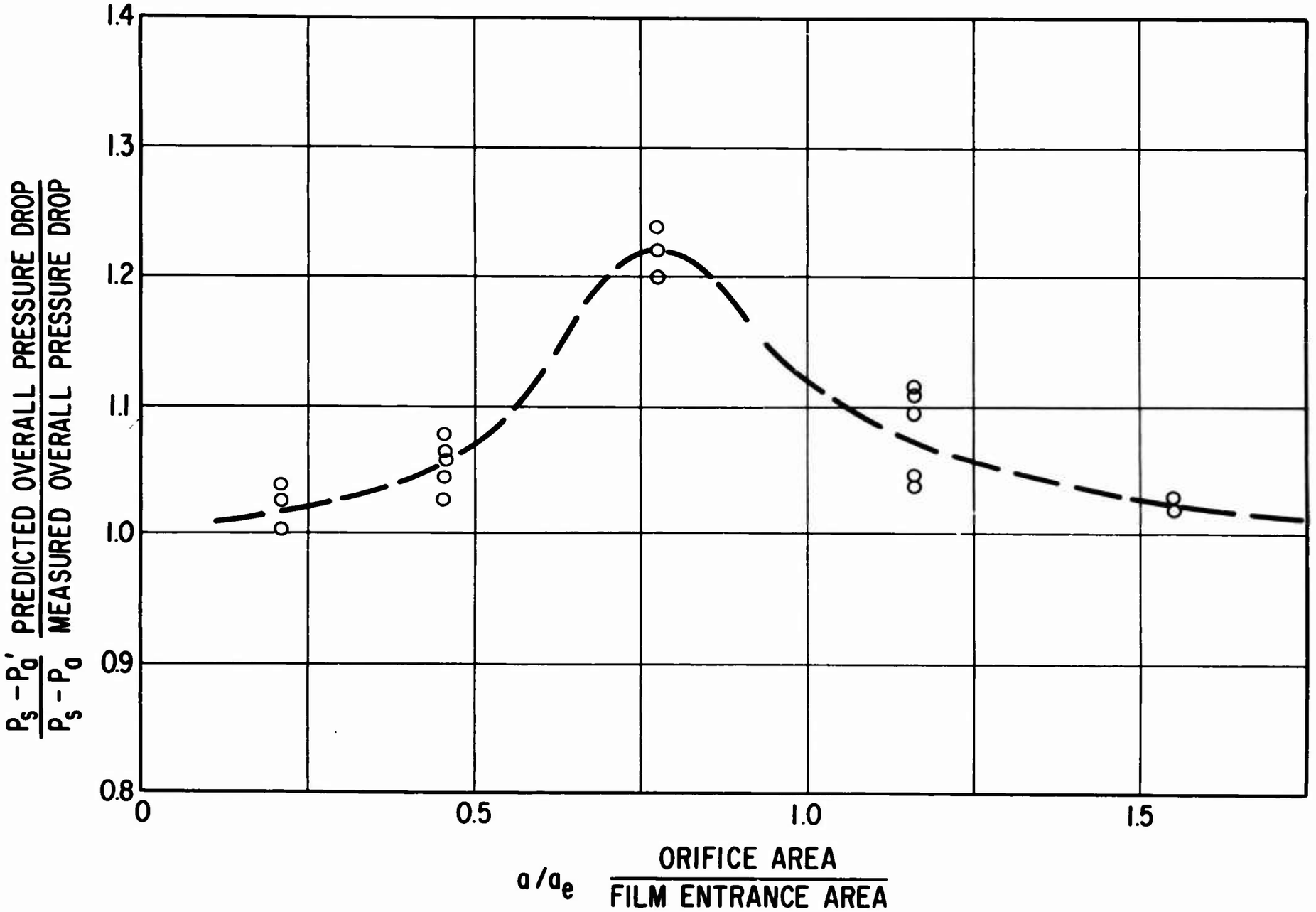

Fig. 19 Accuracy of Calculated Overall Bearing Pressure Loss Using Uncorrected Film Entrance Loss Coefficients

MTI-1392

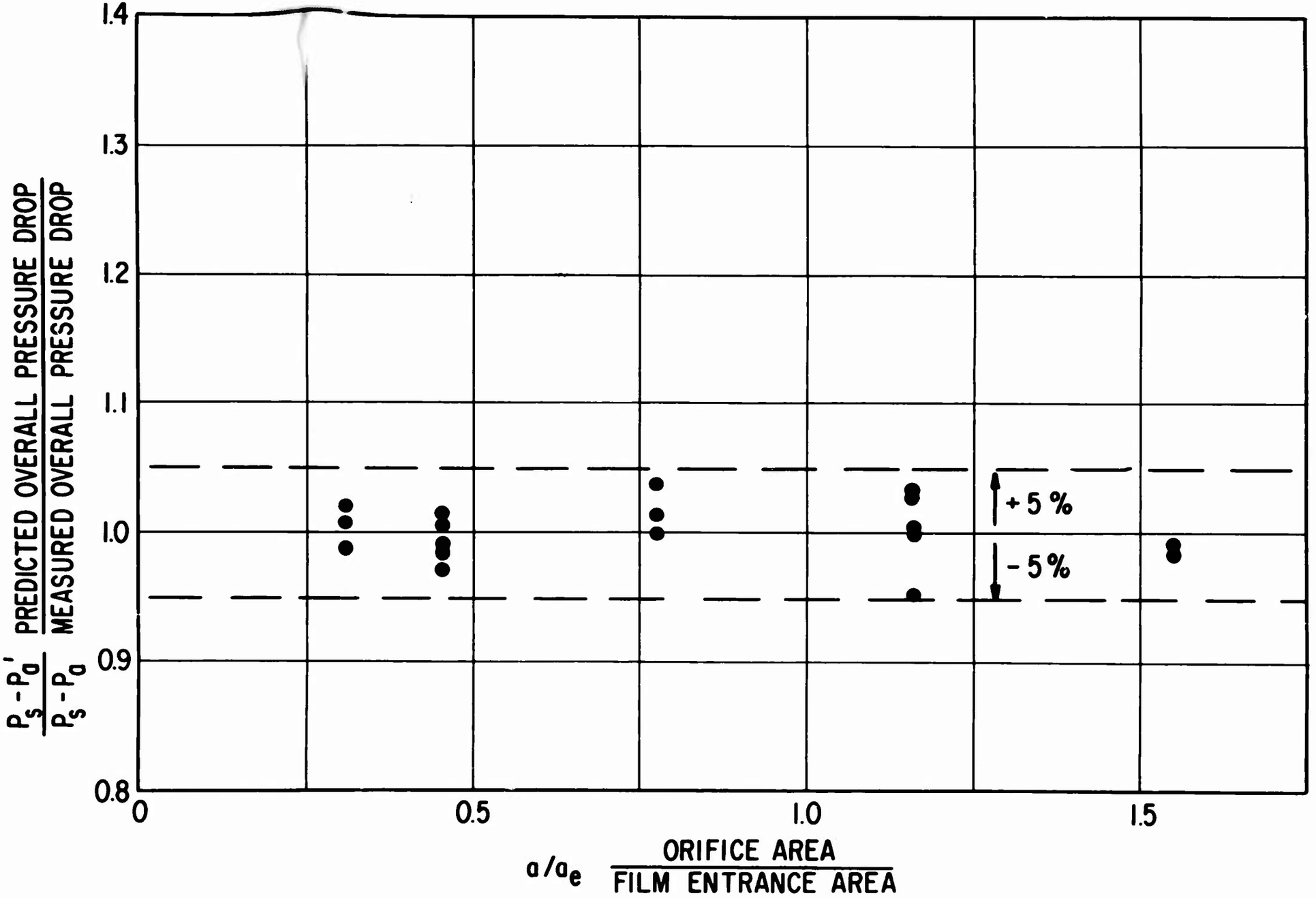

Fig. 20 Accuracy of Calculated Overall Bearing Pressure Loss Using Corrected Approach for Determining Film Entrance Loss

MTI-1393

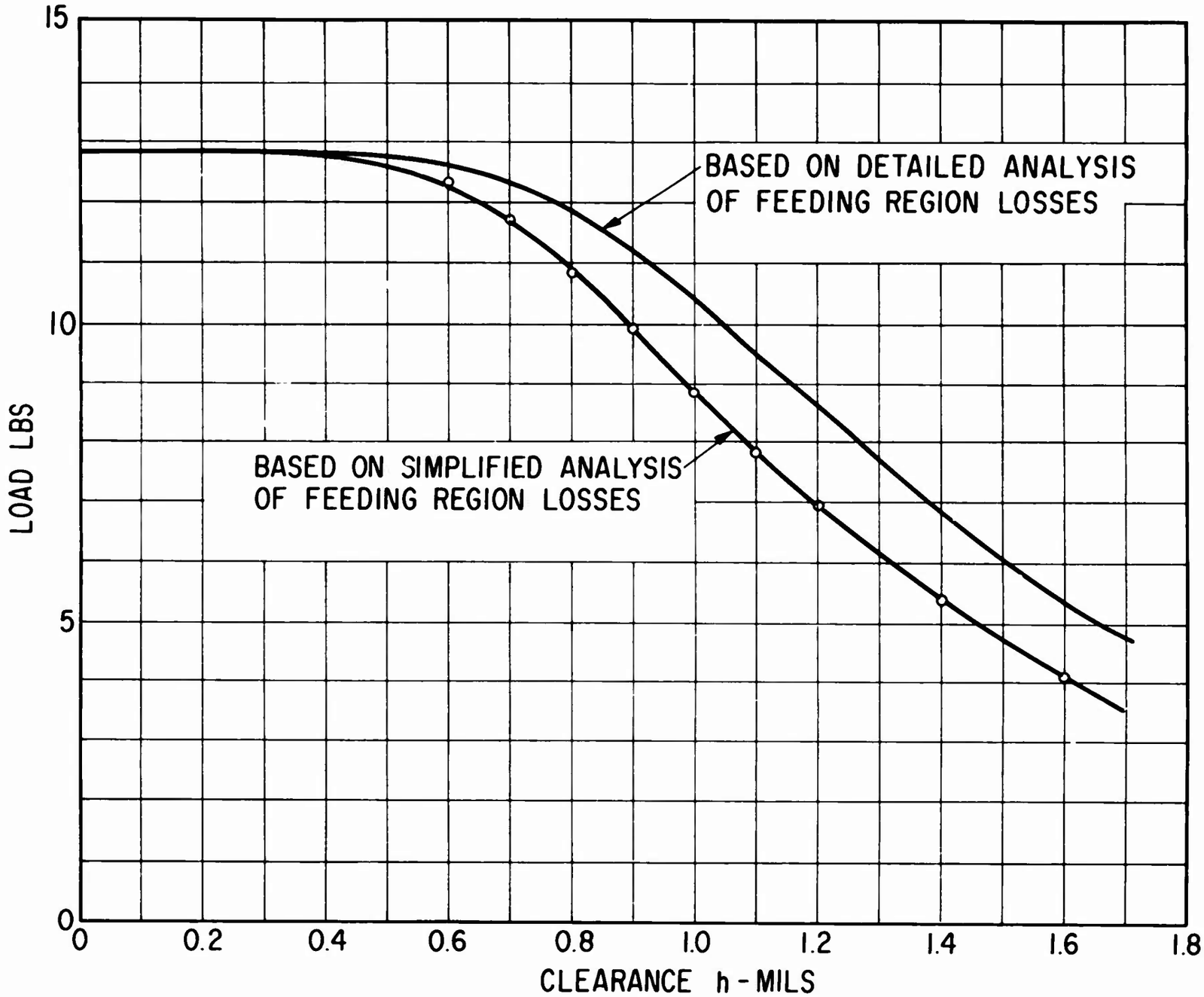

Fig. 21 Comparison of Calculated Bearing Load vs. Clearance Curves

MTI-1394

Fig. 21 Comparison of Calculated Bearing Load vs. Clearance Curves

MTI-1394

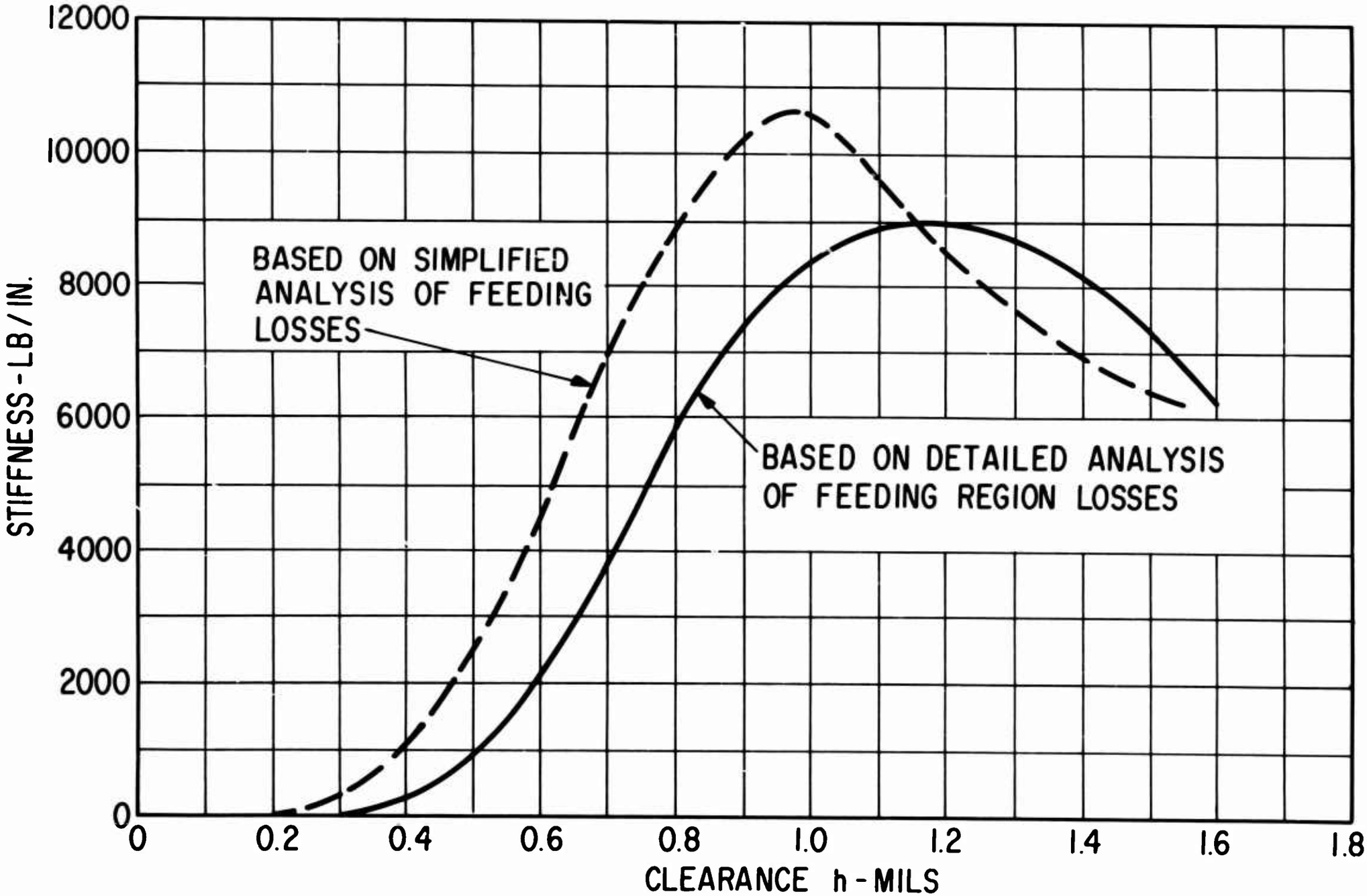

Fig. 22 Comparison of Calculated Stiffness Curves

MTI-1395